Provenance versus weathering control on sediment composition in monsoonal subtropical climate (South China) - 2. Sand petrology and heavy minerals

Eduardo Garzanti[1*], Jie He[1,2*], Marta Barbarano[1], Alberto Resentini[1], Chao Li[1,3], Lu Yang[1,4], Shouye Yang[4], Hua Wang[2]

[1] Laboratory for Provenance Studies, Department of Earth and Environmental Sciences, University of Milano-Bicocca, Milano 20216, Italy

[2] School of Earth Resources, China University of Geosciences, Wuhan 430074, China

[3] State Key Laboratory of Mineral Deposit Research, School of Earth Sciences and Engineering, Nanjing University, Nanjing 210023, China

[4] State Key Laboratory of Marine Geology, Tongji University, Shanghai 200092, China

Email addresses: eduardo.garzanti@unimib.it, jiehe19920402@163.com, marta.barbarano@unimib.it, alberto.resentini@unimib.it, lichao@smail.nju.edu.cn, 13yanglu@tongji.edu.cn, syyang@tongji.edu.cn, wanghua@cug.edu.cn.

Corresponding authors: : eduardo.garzanti@unimib.it and jiehe19920402@163.com,

Key Words: Pearl River; southern Yangtze tributaries; Rivers of Fujian and Zhejiang Provinces; Provenance of Taiwan sandstones; Sediment budgets and erosion rates; Fengcong and fenglin karst; Dissolution of carbonate grains; Durability of detrital minerals; Cathaysia and Yangtze blocks.

ABSTRACT. Together with the companion article dedicated to sedimentary geochemistry and clay mineralogy, this study investigates the interplaying controls on the generation and composition of river sediments across South China. In the Pearl River and southern Yangtze catchments, dominantly sedimentary and basaltic rocks of the Yangtze block shed quartzo-lithic sedimentaclastic sand, whereas mostly granitic and sedimentary rocks of the Cathaysia block generate feldspatho-quartzose sand. Rivers of the Fujian and Zhejiang Provinces draining the SE Coast Magmatic Belt carry feldspatho-litho-quartzose volcaniclastic sand containing epidote with minor clinopyroxene and olivine locally. Within the Pearl River catchment, 35-40% of the sand is derived from the Yangtze block, and 60-65% from the Cathaysia block. Erosion rates are fairly evenly distributed across the basin, reaching higher values in the Hongshui headwaters where topographic relief is greater.

South China hosts one of the largest and most spectacular karst areas on Earth, where two landscape types are characterized by different intensity of chemical dissolution. In *fengcong* (cone) *karst*, carbonate detritus attacked by carbonic and sulfuric acids is partly preserved, whereas carbonate grains are completely dissolved in *fenglin* (tower) *karst* developed in wetter regions to the east. The strong climatic gradient from the dry Tibetan plateau in the west to monsoon-drenched coastal areas is faithfully reflected in illite-rich *vs.* kaolinite-rich clay-mineral assemblages, but in sand the weathering effect is much harder to isolate from the dominant effects of source-rock lithology and recycling. The different durability of tectosilicates (quartz > microcline > orthoclase > plagioclase) or the degree of surficial corrosion displayed by heavy minerals offer complementary information but cannot represent robust proxies for weathering intensity. The *sand generation index* SGI reveals whether lithologies are under- or over-represented in detrital assemblages and proved to be most useful to trace different weathering regimes across South China.

Direct comparison between sand generated today in the Chinese mainland and Taiwan sandstones is prevented because of the diagenetically depleted mineralogical suite of the latter. The relative proportions of durable minerals, complemented by zircon-geochronology data, indicates that Neogene sandstones exposed in western Taiwan were principally fed by a paleo-Yangtze River.

> ”It’s said that there was nothing there until a jewel merchant from across the sea dropped the best of his pearls in the river … It lay at the bottom, glowing like a lantern and slowly growing larger until it grew into an island. And from then on that waterway became famous as the Choo Kiang, or “Pearl River”. *Amitav Gosh, River of smoke, ch. 13*

1. Introduction

The compositional signatures of sand and sandstone are controlled primarily by the mineralogy of parent rocks and secondarily by a range of physical and chemical processes (Johnsson, 1993; Weltje and von Eynatten, 2004). Because of nature’s complexity, there is little chance of finding simple straightforward answers to geological problems if sand detrital modes are used without taking the necessary care to detangle such an intricate system of interplaying factors (Garzanti, 2016; Basu, 2017). Conversely, once we succeed in isolating and understanding the different mark of each, we find in sediment composition a key that unlocks a bounty of information, helping us to investigate a wide range of phenomena. These include tectonic processes in diverse geodynamic environments (Dickinson, 1985; Ingersoll, 2012), the characteristics of weathering in different climatic and geomorphological settings (Nesbitt et al., 1997; von Eynatten et al., 2016), and hydraulic parameters during erosion, transport, or deposition (Garzanti et al., 2008, 2009). To complete this hard passage we need first to gain thorough experience on modern sedimentary systems and next use it as a conceptual guide during our cautious exploration of past conditions.

South China is characterized by a strong climatic gradient from the dry Tibetan plateau in the west to monsoon-drenched coastal areas in the east, with an additional latitudinal rainfall gradient. A most interesting peculiarity of this vast continental region is the extensive exposure of carbonate rocks, which makes its western part one of the world’s largest karst terrains. Because of sharp climatic gradients and varied geological and geomorphological conditions, South China is excellently suited to appraise the relative effect of source-rock lithology and chemical weathering,

as well as other interplaying factors affecting sediment generation and composition. This study focuses on sand produced in the catchments of the Pearl River, of major southern tributaries of the Yangtze River, and of smaller rivers draining the Fujian and Zhejiang Provinces between the Pearl and Yangtze river mouths (Fig. 1).

Our aims are diverse. The characterization of the petrographic and mineralogical signatures in each river catchment allows us to: a) calculate a provenance budget, assess sediment yields, and trace erosion patterns in the Pearl River basin; b) evaluate the extent to which detrital modes are modified by chemical weathering in different climatic conditions; c) investigate the processes that control the dissolution of soluble carbonate grains in different types of karst terrains; d) determine the relative durability of detrital tectosilicates; e) verify whether corrosion features on heavy minerals can be used as a proxy of weathering conditions. Additionally, we touch on the highly controversial topic of provenance and dispersal pathway of Cenozoic Taiwan sandstones fed from the Chinese mainland. To reach these multiple goals, original petrographic and heavy-mineral data are integrated with clay-mineral and geochemical data from the companion paper (He et al., companion), petrographic and heavy-mineral data on Yangtze sand and Neogene to modern sediments of western Taiwan (Nagel et al., 2014; Vezzoli et al., 2016; Resentini et al., 2017), and zircon-geochronology data from river sand in mainland China and Taiwan (Xu et al., 2007; He et al., 2013; Xu et al., 2014, 2016; Zhao et al, 2015; Deng et al., 2017; Liu et al., 2017; Zhong et al., 2017; He et al., 2019). Previous heavy-mineral studies on sand carried by the Pearl River and smaller rivers of coastal SE China include those of Xu and Li (2003), Xiang et al. (2011), Chen et al. (2018), and Ma et al. (2018).

2. Geology and geomorphology

The South China block consists of the Yangtze block to the north and the Cathaysia block to the south, welded by the early Neoproterozoic Jiangnan orogen (Fig. 2; Shu et al., 2011; Yao et al.,

2016). The timing and location of the suture zone are however disputed, as in general the complex pre-Devonian geological evolution of southern China (Wang et al., 2007; Li et al., 2009; Zhao and Cawood, 2012; Li et al., 2014).

Basement rocks of the Yangtze block are as old as Mesoarchean to Paleoproterozoic (Qiu et al., 2000; Wang et al., 2012) but are rarely exposed, whereas widely distributed are upper Paleozoic carbonates overlain by the Permian Emeishan Traps, representing the largest igneous province in China. The thickness of basaltic flows increases from 200 m in the Guizhou Province to as much as 5 km in the west, being ~700 m on average (Shellnutt, 2014). Carbonate sedimentation continued into the Triassic, replaced by siliciclastic strata during the Late Triassic to Jurassic (Liu and Xu, 1994).

The Paleoproterozoic basement core of the Cathaysia block, as old as ~2 Ga and consisting of granitoid gneiss and schist presently exposed in SW Zhejiang and NW Fujian (Li, 1997; Wan et al., 2007; Yu et al., 2009; Xia et al., 2012), collided with the Yangtze block between 800 and 900 Ma during the Jiangnan orogeny and was subsequently fragmented in diverse terranes and sedimentary basins hosting thick successions of clastic rocks (Shu, 2006). A major tectonic boundary corresponds to the Zhenghe-Dapu Fault, which separates a SE domain (eastern Cathaysia block) dominated by upper Mesozoic igneous rocks (Xu et al., 2007) from a NW domain (western Cathaysia bock) characterized by a fold-thrust belt formed during the late Ordovician-Silurian Wuyi-Yunkai (Kwangsian) orogeny and unconformably overlain by upper Paleozoic clastic and subordinately carbonate rocks (Li et al., 2010). Western Cathaysia is further subdivided into the Wuyi terrane in the north, drained by the studied rivers of coastal SE China, and the Nanling-Yunkai terrane in the south, drained by lower-course tributaries of the Pearl River (Fig. 2; Yu et al., 2010).

2.1. Pearl River catchment

The Pearl River (Chinese name Zhujiang, from *zhu*, pearl, and *jiang*, river; length 2320 km, catchment area 450,000 km^2) is the third longest river in China, and changes names downstream of each major confluence (Fig. 1). The Nanpan and Beipan headwater branches are sourced in the Yunnan-Guizhou Plateau of southeastern Tibet at an elevation of ~2800 m a.s.l., and flow eastward across the Yangtze block where elevation is >1800 m to join and form the Hongshui River (Table 1). Downstream, the Hongshui (from *hong*, red, and *shui*, water) enters the Cathaysia block, where it takes the name of Qian after the confluence with the Liu River and of Xun after the confluence with the Yu River. In the lower course, it takes the name of Xi (*west* in Chinese) downstream of the confluence with the Gui (Li) and He Rivers, and is eventually joined by the Bei (*north* in Chinese) and Dong (*east* in Chinese) Rivers in the Guangzhou area to form both a delta in the south and an estuary in the north (the Humen, known by Europeans as *Bocca Tigris*).

The Pearl River basin straddles the Tropic of Cancer. The average annual temperature in the catchment ranges between 14°C and 22°C, reaching as low as -10°C and as high as 42°C. Climate is strongly influenced by the East Asia summer monsoon with annual precipitation, concentrated between April and September, increasing steadily from 0.7 m in the west to 2.4 m along the coast (Fig. 3; Zhang et al., 2012; Liu et al., 2016). The estimated mean annual water and sediment fluxes range between 280 and 330 km^3 and between 65 and 86 million tons, respectively (Pearl River Water Resources Commission, 2006).

The Pearl River catchment encompasses diverse geological domains (Fig. 2): a) the upper Middle Permian Emeishan Large Igneous Province in the northwest consists of basalt and minor basaltic andesite, picrite, trachyte, and rhyolite (Song et al., 2001; Shellnutt, 2014); b) the Chuandian fragment in the far west comprises a suite of igneous rocks from small ultramafic bodies and gabbro to granodiorite and granite (Li et al., 2003); c) the Youjiang Structural Belt in the west includes deformed Cambro-Ordovician carbonates unconformably overlain by Devonian to Middle Triassic carbonates and siliciclastic rocks (Yang et al., 2012; Li et al., 2017); d) the North Vietnam terrane

in the southwestern corner of the catchment comprises Neoproterozoic metasedimentary and igneous basement intruded by Silurian granitoids, and Paleozoic–Mesozoic sedimentary and volcano-sedimentary cover strata (Yang et al, 2012); e) the Jiangnan orogen in the north consists of Neoproterozoic schist and minor granite (Li, 1999; Wang et al., 2014); f) the Shiwandashan Structural Belt in the south contains Paleozoic-Mesozoic siliciclastic strata with Triassic granitoid intrusions (Hu et al., 2015; Li et al., 2017); g) the Yunkai Massif, also in the south, includes amphibolite-facies to granulite-facies metamorphic rocks deformed during the Early Paleozoic Wuyi-Yunkai orogeny (Wang et al., 2013); h) the SE Coast Magmatic Belt contains widespread Jurassic to Cretaceous Yanshanian granitoids with high-K calc-alkaline affinity (Chen et al., 2008).

The Hongshui and Yu headwater branches of the Pearl River drain the Yangtze block in the western part of the catchment, where upper Paleozoic carbonates, Emeishan basalts, and Triassic dolomites and continental redbeds are widely exposed (Fig. 4; Chen and Pei, 1993). The Rong tributary of the Liu River is sourced in the Jiangnan orogen in the north. All Pearl River tributaries in the eastern catchment drain entirely within the Cathaysia block, characterized by Paleozoic limestones and subordinate siliciclastic strata in the west (Gui and He catchments) and by Yanshanian granites in the east with Paleozoic carbonates (Bei catchment) or Jurassic sandstones and mudrocks (Dong catchment) (Jahn et al., 1990).

2.2. Coastal SE China

The Fujian and Zhejiang Provinces of SE China at latitudes between 24°N and 30°N have subtropical climate dominated by the East Asia monsoon, with average annual temperatures of 17-21°C. Annual precipitation increases southward from 1.6 to 2.2 m (Fig. 3). Several rivers drain eastward across this hilly region characterized by elevations between 500 and 1000 m. The largest is the Min River, which annually delivers ~56 km^3 of water and ~8 Mt of suspended sediment to the Taiwan Strait (Table 1).

All coastal rivers drain entirely within the Cathaysia block, the SE part of which largely consists of granite and volcanic rocks with ages younging eastward from Jurassic to Cretaceous (Fig. 4; Zhou et al., 2006; Li and Li, 2007). The rhyolite-dominated bimodal volcanic suite including minor basalt and mafic dykes is distributed over 800 km in the so-called SE Coast Magmatic Belt, and documents the late stages of westward subduction of the paleo-Pacific plate beneath the South China block with subsequent crustal thinning and incipient back-arc extension in the South China Sea (Chen et al., 2008). Jurassic-Paleogene siliciclastic rocks intercalated with rhyolitic ignimbrites and deposited during this subduction-related, Basin-and-Range-type upper-plate extension widely occur in coastal areas (Wang and Shu, 2012).

In the northwestern Wuyi terrane, deformed Cambrian feldspatho-quartzose metasandstones and slates are overlain with angular unconformity by a ~3.5 km-thick upper Paleozoic succession dominated by quartz-rich sandstone and conglomerate intercalated with mudrock and bioclastic limestone (Fujian Institute of Geological Survey, 2015). The occurrence of granitoid intrusions and volcanic detritus in the Lower Permian has suggested a continental-arc setting related to the initial westward subduction of the paleo-Pacific plate (Li et al., 2020).

2.3. Southern Yangtze catchment

The Yangtze (Chinese name Changjiang, from *chang*, long and *jiang*, river) is the largest river in China. The southern part of its huge catchment, with mean annual temperature 16-18°C, is situated in the humid subtropical zone influenced by the East Asia monsoon. Annual precipitation, concentrated from May to October, increases from 0.6-1.2 m in the Wu catchment, where elevation is 500-2000 m a.s.l., to 1.2-2.5 m in the Yuan, Xiang and Gan catchments lying mostly below 500 m a.s.l. (Fig. 3).

The Wu River drains entirely within the Yangtze block, including mostly upper Paleozoic to Triassic carbonates with coal-bearing strata and basalt in the upper reaches and mudrocks with sporadic Neoproterozoic greenschist-facies volcano-sedimentary rocks in the lower reaches. The

other three tributaries to the east drain Neoproterozoic schist and granite of the Jiangnan orogen (from *jiang* = river, and *nan* = south; i.e., "located south of the river"), overlain by middle-upper Neoproterozoic (Sinian) siliciclastic cover locally including stromatolitic dolostone (Wang et al., 2007; Zhao, 2015). The Yuan River drains both sedimentary rocks of the Yangtze block and middle Neoproterozoic schist of the Jiangnan orogen. The Xiang and Gan tributaries (Table 1) are sourced in the northern part of the Cathaysia block and cut across the Jiangnan orogen including granite, schist, and mostly siliciclastic sedimentary cover (Fig. 4).

2.4. Western Taiwan

Taiwan Island, located between ~22°N and ~25°N, has mild tropical climate through the year, with average annual temperature from 22°C to 24°C; summer temperatures reach 38°C, whereas frost or snow may cover the high mountains during winter. Annual rainfall, concentrated between May and October, increases from 1-1.5 m along the western coast to the northern foothills and central high-mountain area, which receive up to 5-6 m of annual precipitation. Typhoons may bring more than 2 m of torrential rain in two days, triggering multiple landslides (Hovius et al., 2000; Montgomery et al., 2014). Because of such harsh climatic conditions coupled with rapid tectonic deformation, extreme relief, and frequency of high-magnitude earthquakes, erosion rates are among the highest on Earth, averaging 3–7 mm/a and reaching several cm/a locally (Dadson et al., 2003; Fuller et al., 2006; Resentini et al., 2017). Sediment geochemistry and clay-mineral assemblages dominated by illite and chlorite testify to the prevalence of physical erosion with limited weathering effects (Liu et al., 2008; Nagel et al., 2014; Garzanti and Resentini, 2016).

The Tsengwen, Bazhang, and Houlong rivers (Table 1) carry detritus entirely recycled from Neogene strata along the western front of the Taiwan orogen. Exposed in the western foothills are sandstones and mudrocks originally accumulated offshore of the SE China coast during opening of the South China Sea and derived from the Chinese mainland in the west, overlain by Plio-Quaternary foreland-basin deposits fed from the growing Taiwan orogen in the east (Lin et al.,

2003; Nagel et al., 2013). The basal unconformity of the foreland basin corresponds to a sharp change in sandstone composition from quartzose in the Miocene to litho-feldspatho-quartzose metasedimentaclastic in the Pliocene, and finally feldspatho-litho-quartzose sedimentaclastic in the Pleistocene, documenting the progressive frontal accretion of unmetamorphosed thrust sheets during the outward growth of the orogen (Nagel et al., 2014).

3. Sampling and analytical methods

For this study, we have selected 40 samples overall (Fig. 1), including 22 very fine to medium sands collected between summers 2018 and 2019 from various tracts and tributaries of the Pearl River, 10 very fine to coarse sands collected mainly in March to November 2011 from five coastal rivers in SE China (Ou, Min, Mulanxi, Jiulong, Han) and their main tributaries, sample #23 collected at 105 b.s.l. offshore of the Pearl River mouth, and one sample each from the four major southern tributaries of the Yangtze River (Wu, Yuan, Xiang, and Gan) and from three selected rivers in western Taiwan (Tsengwen, Bazhang, and Houlong). Full information on sampling sites (numbered from 1 to 40 in Figs. 2 and 3) is given in Appendix Table A1 and in the Google Earth™ file PearlProv.kmz.

3.1. Petrography

A quartered fraction of each sand sample was impregnated with araldite epoxy and cut into a standard thin section stained with alizarine red to distinguish dolomite and calcite. Petrographic analysis was carried out by counting between 400 and 500 points under the microscope according to the Gazzi-Dickinson method (Ingersoll et al., 1984). Sand classification was based on the relative abundance of the three main framework components quartz (Q), feldspars (F) and lithic fragments (L), considered if exceeding 10%QFL. According to standard use, the less abundant component goes first, the more abundant last (e.g., a sand is named feldspatho-litho-quartzose if Q > L > F >

10%QFL or quartzo-lithic if L > Q > 10%QFL > F; classification scheme after Garzanti, 2019). Quartz-rich feldspatho-quartzose (4 < Q/F < 9) and quartz-rich litho-quartzose subfields (4 < Q/L < 9) are also distinguished. Metamorphic grains were classified according to their protolith composition and metamorphic rank (Garzanti and Vezzoli, 2003). Petrographic parameters used in this article include the Q/F, P/F, and Mic*/F ratios (P = plagioclase; Mic* = microcline with cross-hatch twinning, called for brevity microcline* through the text). Median grain size was determined in thin section by ranking and visual comparison.

3.2. Heavy minerals

From a split aliquot of the 15-500 μm size window (32-355 μm for Yangtze tributaries and 32-500 μm or bulk sample for Taiwan rivers) obtained by wet sieving, heavy minerals were separated by centrifuging in Na-polytungstate (2.90 g/cm^3) and recovered by partial freezing with liquid nitrogen. For each sample, ~200 transparent heavy minerals (or all of those present in the grain mount) were either point-counted at appropriate regular spacing to obtain correct volume percentages or grain-counted by the area method (Galehouse, 1971). Transparent heavy-mineral assemblages, called for brevity "tHM suites" throughout the text, are defined as the spectrum of detrital extrabasinal minerals with density >2.90 g/cm^3 identifiable under a transmitted-light microscope. According to the transparent-heavy-mineral concentration in the sample (tHMC), tHM suites are defined as very poor (tHMC <0.5), poor (0.5 ≤ tHMC <1), moderately poor (1 ≤ tHMC <2), or moderately rich (2 ≤ tHMC <5) (Garzanti and Andò, 2019). The sum of zircon, tourmaline, and rutile over total transparent heavy minerals (ZTR index of Hubert, 1962) measures the relative proportion of durable minerals in the tHM suite and can thus be used as an index of recycling (Garzanti, 2017).

In all analysed samples, corrosion features were systematically evaluated on ~ 5300 transparent heavy-mineral grains, following the classification of surface textures in Andò et al. (2012). The

Corrosion Index CI = [(etched grains +50% corroded grains) / total grains × 100] could thus be defined for each mineral (Garzanti et al., 2018). The Raman spectra of 38 garnet grains separated by hand-picking from Ou, Min, Jiulong, and Han sand samples were obtained with a Renishaw inVia™, and their chemical composition was recalculated from Raman peak wavenumbers elaborated by the Matlab® routine MIRAGEM (Bersani et al., 2009). Significant detrital components are listed in order of abundance (high to low) throughout the text. Key compositional parameters are summarized in Table 2. The complete petrographic and heavy-mineral datasets are provided in Appendix Tables A2, A3, and A4.

3.3. Statistical/graphical displays and chemical indices

The compositional biplot (Gabriel, 1971), drawn using CoDaPack software by Comas-Cufí and Thió-Henestrosa (2011) and used to illustrate integrated petrographic, heavy-mineral, and geochemical data, allows discrimination among multivariate observations (points) while shedding light on the mutual relationships among multiple variables (rays). The length of each ray is proportional to the variance of the corresponding variable in the dataset. If the angle between two rays is close to 0°, 90° or 180°, then the corresponding variables are directly correlated, uncorrelated, or inversely correlated, respectively.

Literature data on zircon ages are visualized as kernel density estimates (KDE) and as multidimensional-scaling (MDS) maps, plotted using the *provenance* package of Vermeesch et al. (2016). In a MDS map, the distance among samples is approximately proportional to the Kolmogorov-Smirnov dissimilarity of their compositional or chronological signatures (Vermeesch, 2013; Vermeesch and Garzanti, 2015). Closest and second-closest neighbours are linked by solid and dashed lines, respectively, and the goodness of fit is evaluated using the "stress" value of the configuration (0.2 = poor; 0.1 = fair; 0.05 = good; Vermeesch, 2018).

Used in this article are the Chemical Index of Alteration [CIA = 100 · $A1_2O_3$ / ($A1_2O_3$ + (CaO - 3.33 P_2O_5) + Na_2O + K_2O)] (Nesbitt and Young, 1982) and the Weathering Index [WIP = 100 · ((CaO -

3.33 P_2O_5) / 0.7+ 2 Na_2O / 0.35 + 2 K_2O / 0.25 + MgO / 0.9)] (Parker, 1970), calculated using molecular proportions of mobile alkali and alkaline earth metals corrected for CaO in apatite. Weathering intensities are calculated separately for each single mobile element *E* by comparing its concentration to that of non-mobile Al in our samples and in the Upper Continental Crust [$\alpha^{Al}E$ = $(Al / E)_{sample} / (Al / E)_{UCC}$] (Garzanti et al., 2013; UCC standard after Taylor and McLennan, 1995; Rudnick and Gao, 2003). None of these indices can be confidently used as a proxy of weathering conditions, because they depend primarily on the lithology of source rocks and on other factors as well, including grain size and hydraulic sorting (Garzanti and Resentini, 2016; Dinis et al., 2020). Because the addition of quartz grains *via* recycling of parent sandstones directly affects the WIP, but not the CIA, the CIA/WIP ratio can be considered as an index of recycling (Garzanti et al., 2014).

4. PETROGRAPHY AND HEAVY MINERALS

In this section we first illustrate the petrographic and heavy-mineral signatures of modern sand generated in the Pearl River catchment and in coastal SE China. Next, we summarize data previously collected with the same methods and following the same criteria on modern river sand from southern Yangtze tributaries (Vezzoli et al., 2016) and western Taiwan (Garzanti and Resentini, 2016; Resentini et al., 2017), and on Miocene-Pleistocene sandstones of the outer western Taiwan foothills (Nagel et al., 2014).

4.1. Headwater Pearl River tributaries

Sand carried by Pearl River tributaries draining the Yangtze block ranges from quartzo-lithic (Hongshui catchment) to litho-quartzose (Yu catchment) and from feldspatho-litho-quartzose to quartz-rich litho-quartzose (Liu catchment) (Fig. 5A). The P/F ratio is varied, with subequal amounts of K-feldspar and plagioclase overall. Feldspars, including common microcline*, are most

frequent in Rong sand, partly derived from basement rocks of the Jiangnan orogen. In the Hongshui catchment, mafic and subordinately felsic volcanic grains are mostly derived from the Emeishan Traps, limestone grains from extensive Upper Paleozoic to Triassic carbonates, and siltsone/metasiltstone to shale/slate grains from siliciclastic rocks. Felsic and mafic volcanic rock fragments occur in You River sand but are diluted in Yu sand downstream, whereas only felsic volcanic grains derived from the Jiangnan orogen occur in Liu sand. Limestone rock fragments associated with some dolostone and chert are common in Yu sand, whereas Rong sand contains significant metamorphic rock fragments and muscovite shed by schists of the Jiangnan basement. Mica is otherwise negligible. Siltsone/metasiltstone to shale/slate grains are subordinate but widespread.

The mostly very poor tHM suites reflect provenance dominantly from carbonate and terrigenous sedimentary rocks. Clinopyroxene (largely brown augite) derived from the Emeishan Traps dominates the tHM suite in Beipan and You sand, and is diluted but still abundant in Hongshui and Yu sand downstream. Amphibole (actinolite with subordinate hornblende) shed from Jiangnan schists is most abundant in Long and Rong sand and is diluted but still common in Liu sand downstream. ZTR minerals are widespread. Tourmaline is most common in Rong and Liu sand, and zircon in Zuo sand, whereas rutile is invariably rare. Epidote is also widespread, and most common in Liu sand. Apatite is abundant in the Nanpan tributary sample but otherwise minor to rare. Minor garnet occurs in Zuo sand. Olivine was detected in You sand, Cr-spinel in Zuo sand, and topaz in Rong, Long, and Liu sand. Other minerals include titanite, anatase, brookite, and pumpellyite. Corrosion indices are higher for amphibole than for pyroxene − but only pyroxene grains may be deeply etched − and low for epidote and other minerals (Table 2).

4.2. Lower-course Pearl River tributaries

Sand carried by Pearl River tributaries draining the Cathaysia block is feldspatho-quartzose or locally litho-feldspatho-quartzose (Gui and upper Bei sand) (Fig. 5A). K-feldspar, including

common microcline*, is twice as abundant as plagioclase. Rock fragments derived from granitoid and mostly metasedimentary rocks occur in all samples. Felsitic volcanic rock fragments occur in Gui, Dong, lower Bei, and He sand. Sedimentary rock fragments are most common in Gui sand (siltstone, shale, limestone, chert) and frequent in upper Bei sand (siltstone), but otherwise negligible. Mica (muscovite ≈ biotite) is common.

The very poor tHM suites include mainly amphibole (green brown to subordinately blue/green hornblende) with epidote, tourmaline, and zircon. The ZTR index ranges from 8 (He sand) to 47 (Xinxing sand). Andalusite mostly showing unoriented carbonaceous inclusions is abundant in Dong sand, where it is associated with fibrolitic sillimanite, and minor in He and Bei sand. Some garnet, associated with staurolite and kyanite in Xinxing sand, and pyroxene (mainly brown augite) invariably occur. Other minerals include titanite, anatase, apatite, rutile, topaz, and monazite. Corrosion indices are only slightly higher than in headwater branches (Table 2), but deeply etched to skeletal amphibole or locally apatite occur.

4.3. The Pearl River mainstem

Xi river sand is litho-feldspatho-quartzose (Fig. 5A) with K-feldspar ≈ plagioclase. Rock fragments are mainly sedimentary to very low-rank metasedimentary (siltstone/metasiltstone, shale/slate, limestone and rare dolostone and chert) and subordinately metamorphic (mainly low-rank metasedimentary) and granitoid types, with minor lathwork and felsitic volcanic grains. Mica (muscovite ≈ biotite) is common. The very poor tHM suite consists of epidote, amphibole (blue/green to green/brown hornblende and actinolite), tourmaline, zircon, and clinopyroxene (mainly brown augite). Other minerals include anatase, apatite, titanite, and locally barite, rutile, monazite, garnet, and prehnite. From the Qian River to the Xi River downstream, quartz, metamorphic rock fragments, mica, and amphibole progressively increase at the expense of sedimentary and especially mafic volcanic rock fragments.

In the Pearl River delta, estuary, and shelf, composition ranges from litho-feldspatho-quartzose for very fine sand to feldspatho-quartzose for fine sand (Fig. 5A). K-feldspar is ≥ plagioclase; microcline* is minor. Metamorphic and sedimentary rock fragments (mostly siltstone/metasiltstone, shale/slate, schist, and very-low-rank to low-rank metavolcanic grains) prevail over granitoid and minor volcanic (mainly felsitic), limestone or chert grains. Mica (biotite > muscovite) is most common in estuary sand. The very poor tHM suite consists of tourmaline, zircon, clinopyroxene (mainly brown augite), amphibole (mostly blue/green hornblende with green/brown hornblende and actinolite), epidote, and locally frequent apatite and garnet. Other minerals include anatase or andalusite; one grain of olivine was identified. Shelf sand is richer in epidote and amphibole, and poorer in clinopyroxene. Corrosion indices, relatively low in the Qian tract (CI 60 for amphibole, 7 for pyroxene, and 6 for epidote), tend to irregularly increase downstream reaching higher values in estuary and shelf sand (up to CI 74 for amphibole, 23 for pyroxene, and 39 for epidote).

4.4. Coastal rivers of SE China

Coastal rivers in SE China drain the Cathaysia block. Sand ranges from feldspatho-litho-quartzose to feldspatho-quartzo-lithic in the Ou and Min catchments in the north, is litho-feldspatho-quartzose in the Mulanxi catchment, and ranges from feldspatho-quartzose to quartzose in the Jiulong and Han catchments in the south (Fig. 5A). Plagioclase prevails over K-feldspar in Ou, Min and Mulanxi sand, where microcline* is scarce, whereas K-feldspar prevails over plagioclase in sand of Jiulong and Han tributaries where microcline* is more common. Mostly felsitic volcanic rock fragments are abundant in the Ou catchment, common in the Min and Mulanxi catchments, and minor in the Jiulong and Han catchments. Granitoid rock fragments are common especially in Mulanxi and Jiulong sand. Other rock fragments include schist (Mulanxi sand) and mainly low-rank metasedimentary and felsic to mafic metavolcanic types, as well as shale/siltstone grains. Carbonate rock fragments are lacking. Biotite and muscovite are common in Ou, Min, and Mulanxi sand.

Very poor to moderately rich tHM suites are epidote-dominated with amphibole, zircon and minor garnet in Ou, Min, and Mulanxi sand, very poor to moderately poor and dominated by epidote and amphibole with locally common zircon and garnet in the Jiulong catchment, and very poor with zircon, amphibole, epidote, tourmaline, and garnet in Han sand. Blue/green hornblende is the most common amphibole. Garnet grains are mainly spessartine associated with andradite and uvarovite in Jiulong sand, almandine and spessartine in Ou sand, and andradite in Han sand. Other heavy minerals include brown augite in Min sand, andalusite (mainly grains free of carbonaceous inclusions in Min sand), titanite, apatite, rutile, olivine, hypersthene, sillimanite, and topaz. Corrosion indices tend to be slightly higher than in the Pearl River catchment (Table 2).

4.5. Southern Yangtze tributaries

Sand of the Wu River, chiefly draining sedimentary rocks of the Yangtze block are quartzo-lithic sedimentaclastic with few feldspars (plagioclase ≈ K-feldspar) and common sandstone/siltstone, shale, limestone, chert, dolostone, and felsic to mafic volcanic rock fragments. Mica is negligible. The very poor tHM suite consists of amphibole (actinolite and hornblende), epidote, augitic clinopyroxene, zircon, garnet, and barite.

Sand of the Yuan River, largely draining the Jiangnan orogen and its mainly siliciclastic cover strata, is litho-quartzose with minor feldspars (plagioclase ≥ K-feldspar, including rare microcline*) and mainly sandstone/siltstone and shale rock fragments associated with felsic volcanic and mostly very-low-rank to medium-rank metasedimentary grains. Limestone grains are rare. Biotite occurs. The very poor tHM suite chiefly consists of zircon, epidote, amphibole (hornblende, actinolite), and tourmaline.

Coarse-grained sand of the Xiang and Gan rivers draining both the Cathaysia block and the Jiangnan orogen are, respectively, quartz-rich feldspatho-quartzose and feldspatho-quartzose. K-feldspar including microcline* predominates over plagioclase (Table 2) Granitoid and siltstone/sandstone rock fragments are associated with a few volcanic, shale, chert, and medium-

rank metamorphic grains. Biotite occurs. Very poor tHM suites include tourmaline and zircon, with subordinate epidote, amphibole (mostly hornblende), locally common topaz, minor garnet, and rare clinopyroxene, rutile, and andalusite. Corrosion indices for sand of Yangtze tributaries are markedly higher than in the Pearl River catchment and coastal rivers of SE China (Table 2), which is however chiefly ascribed to inter-operator bias.

4.6. Taiwan river sands and Neogene sandstones

Sand carried by the Tsengwen, Bazhang, and Houlong rivers, selected because they exclusively drain Neogene strata exposed in the outer western Taiwan foothills, are litho-quartzose to feldspatho-litho-quartzose. Plagioclase prevails over K-feldspar, which may include significant microcline*. Rock fragments are dominantly sedimentary (siltstone and shale, with subordinate limestone and marl) but felsitic volcanic, slate, metasiltstone, and a few granitoid grains frequently occur. The very poor tHM suite include zircon, garnet, epidote, tourmaline, apatite, rutile, minor amphibole, and sporadic augite.

Mid-Miocene to Pleistocene sandstones of the outer western Taiwan foothills are mainly litho-feldspatho-quartzose with subequal K-feldspar and plagioclase. Rock fragments are dominantly sedimentary to low-rank metasedimentary (shale/slate, siltstone/metasiltstone) with minor volcanic grains. Bioclasts are locally abundant. Very poor tHM suites include zircon, tourmaline, garnet, epidote, apatite, and rutile.

5. Provenance control on sand composition

The area investigated in this study covers the whole of southern China south of the Yangtze River. The geology of this large region is complex, comprising the Archean Yangtze (Wang et al., 2012) and Paleoproterozic Cathaysia (Li, 1997) crustal blocks, the early Neoproterozoic Jiangnan orogen that welded them (Yao et al., 2016), as well as the late Ordovician-Silurian Wuyi-Yunkai thrust belt

(Li et al., 2010), the Triassic Indosinian orogen (Hu et al., 2015), and the SE coastal belt characterized by Basin-and-Range-style Jurassic-Cretaceous tectonics and magmatism (Li and Li, 2007; Wang and Shu, 2012). Despite the variety of source rocks, sediments produced in this vast area display two main compositional signatures: quartzo-lithic sand generated by erosion of sedimentary and basaltic cover rocks of the Yangtze block, and feldspatho-quartzose sand generated by erosion of igneous and sedimentary rocks of the Cathaysia block. Virtually all studied sands have poor, and mainly very poor tHM suites with common durable minerals (ZTR mainly ≥ 30), reflecting the dominance of sedimentary and granitic rocks with only sporadic exposure of denser – and consequently dense-mineral-rich (Garzanti et al., 2001, 2006) – mid-crustal crystalline basement. Not only sand generated in western Taiwan, but also sediments produced across southern China are thus largely polycyclic.

5.1. The Yangtze block as a source of sand

In the Guizhou and Guangxi Provinces of SW China, basement rocks of the Yangtze block are extensively covered by upper Paleozoic to lower Mesozoic carbonate, basaltic, and siliciclastic rocks. Consequently, the Wu, Hongshui, and Yu Rivers carry lithic-rich sand with subordinate quartz and low feldspar. Quartz grains frequently display abraded overgrowths as direct witnesses of sandstone recycling. Despite the thickness and extent of carbonate rocks, sedimentary rock fragments are mainly siltstone and shale rather than limestone, an issue discussed specifically in section 6. Volcanic detritus from the Emeishan Traps is documented by mainly mafic lathwork grains and common to dominant augitic clinopyroxene in sand of the Beipan River and of the Hongshui River downstream. Composition is similar but richer in quartz in sand of the Yu River and of its You branch upstream, draining the Youjiang Basin where siliciclastic rocks are more common and granite occurs. Basaltic rock fragments are minor, and yet augite derived from the Emeishan Traps may dominate the very poor tHM suite. Quartz and feldspar increase further in

sand of the Zuo River, partly draining the Vietnam terrane in the southwestern corner of the Pearl River catchment, and of the Rong River, draining Neoproterozoic schists of the the Jiangnan orogen at the northern edge of the catchment. Quartz is most abundant in the Long River and in the Liu River downstream, where quartz grains with abraded overgrowths are particularly common, documenting extensive recycling of quartz-rich sandstones. Conversely, carbonate grains are negligible despite widespread exposure of carbonate rocks, as discussed in section 6

The Wu River, draining cover strata of the Yangtze block north of the Hongshui catchment, carries quartzo-lithic sedimentaclastic sand relative rich in carbonate grains. Instead, the Yuan River, draining both cover strata of the Yangtze block and schists and siliclastic cover strata of the Jiangnan orogen north of the Liu catchment, carries litho-quartzose sand rich in siltstone and shale grains.

5.2. The Cathaysia block as a source of sand

The Cathaysia block comprises diverse geological domains characterized by partly different lithological assemblages and thus shedding detritus with partly different compositional signatures: a) the Yunkai and Nanling terranes in the south; b) the Wuyi terrane in the north, bounded by the Jiangnan orogen farther north; and, c) the SE Coast Magmatic Belt in the east (Fig. 2).

The Xinxing River draining the Yunkai terrane south of the Pearl River, and the He, Bei, and Dong Rivers draining the Nanling terrane north of the Pearl River, all carry feldspatho-quartzose sand with K-feldspar largely prevailing over plagioclase, some metamorphic detritus (low-rank to medium-rank metasedimentary grains and mica), and very poor tHM suites with common hornblende or locally andalusite and other minerals contained in medium-grade metasedimentary rocks (garnet, sillimanite, staurolite, or kyanite). Sand of the Gui and upper Bei Rivers contain a little more carbonate and very-low-rank metasedimentary grains, respectively. Amphibole decreases steadily from west to east. Common andalusite with unoriented carbonaceous inclusions associated

with sillimanite in Dong sand may be derived from graphitic metapelites in the contact aureole of Jurassic-Cretaceous granites (Tong and Tobish, 1996).

Sand shed by the Wuyi terrane and carried by the Han and Jiulong Rivers shares a similar signature. Differences include some more quartz and volcanic rock fragments, and less sedimentary rock fragments. Han sand contains more zircon, and Jiulong sand more epidote. Instead, sand generated in the Mulanxi, Min and Ou catchments farther north is compositionally distinct. Volcanic detritus from the SE Coast Magmatic Belt is testified by felsic volcanic grains, most common in the Ou catchment where volcanic rocks are most abundant (Fig. 4), and by poor, epidote-dominated tHM suites only locally including some clinopyroxene, minor olivine, and rare Cr-spinel.

Although the Xiang and Gan Rivers drain also the Jiangnan orogen in their lowermost course, their sand has detrital modes similar to Jiulong sand and nearly identical to Han sand, indicating that sediment is dominantly generated in the Cathaysia block. Topaz grains, quite common in Xiang sand and frequently detected in sediment generated all across the Cathaysia block from the Liu catchment in the west to the Han catchment in the east, are presumably derived from topaz-bearing peraluminous granites and felsic subvolcanic rocks of both Late Triassic (Indosinian) and Jurassic-Cretaceous (Yanshanian) ages, peculiar of SE China and typically associated with tungsten and tin ore deposits (Ottens and Cook, 2005; Yu et al., 2007).

5.3. Sediment budget and erosion rates in the Pearl River catchment

Within a drainage basin, the relative sediment contribution from different geological units or different tributaries (i.e., provenance budget) can be assessed by forward mixing calculations based on a complete set of petrographic and mineralogical data (method and pitfalls illustrated and discussed in Garzanti et al., 2007, 2012). If information on gauged sediment loads is available, then sediment yields from different geological units or different tributaries (i.e., sediment budget) and an average erosion rate in each catchment can be estimated. The procedure, largely empirical and based on a series of untested assumptions, suffers from several

sources of uncertainty. The major source of error stems from chronically incomplete and inaccurate data on sediment loads, and especially on bedload that is generally roughly considered to represent ~5-10% of suspended load on average (Milliman and Farnsworth, 2013 p.24).

In theory, the proportional supply from diverse sediment sources can be robustly constrained whenever the signature of each source is sufficiently well differentiated by a wide set of compositional parameters. In practice, the accuracy of results is limited by a variety of factors. These include grain-size-dependent or seasonal variability of sediment composition in each river, selective loss of mechanically (e.g., shale) or chemically (e.g., carbonate) labile grains during sediment generation and transport, hydraulic-sorting effects during erosion, transport and deposition, irregular distribution in time and space of easily eroded recent deposits (e.g., landslides, terraces, moraines), imperfect sediment mixing and homogenization along the river, field sampling or laboratory procedures failing to satisfying in full requirements of reproducibility and representativeness, and errors during analysis. Only a few of these undesired effects can be tested. Moreover, data on sand can be extrapolated to the entire sediment flux only under the fragile assumption that mud is supplied in the same proportion as sand in each catchment.

Uncertainties can be minimized by collecting replicate samples especially in the deltaic region, and by performing multiple series of calculations according to a range of plausible criteria which simultaneously satisfy best-fit conditions for diverse successive tracts of the river system (e.g., Vezzoli et al., 2020). In the Pearl River, we analysed four samples along the Qian, Xun, and Xi tracts, and four samples with different grain size in the delta and estuary. Nevertheless, because of the marked compositional variability observed in the coastal region, characterized by a very complex network of distributaries, the mineralogical signature of sediment delivered to the South China Sea could not be assessed precisely.

With these limitations, we calculated that 35-40% of Pearl River sand is generated from mostly sedimentary and mafic volcanic rocks of the Yangtze block in the western upstream reaches, and 60-65% from mostly felsic igneous and sedimentary rocks of the Cathaysia block in the eastern reaches. Sand is contributed in similar amount from each major tributary (~15% from the Hongshui, and 10-15% each from the Yu, Liu, Gui, He, Bei, Dong). Based on gauged suspended-load data (Table 1), and on the assumptions that grain density is 2.67 g/cm^3 as indicated by mineralogical data (SRD index of Garzanti and Andò, 2007) and that bedload represents 10% of suspended load, the annual sediment yield and erosion rate averaged across the catchment are assessed as 160-210 t/km^2 and 0.06-0.08 mm, respectively. Forward mixing calculations and suspended-load data converge to indicate that erosion rates are distributed rather evenly, ranging mostly between 0.05 and 0.1 mm/a and reaching slightly higher values in the headwaters where topographic relief is greater (up to ~0.2 mm/a in the Beipan catchment) (Table 1). Extensive chemical erosion in carbonate-dominated areas, as discussed in section 6, contributes to reduce solid sediment supply to the South China Sea.

5.4. Evaluating polycyclicity

Although it has long been known that a large percentage of sand is generated by recycling of parent sandstones, estimating the relative amount of polycyclic detritus proves to be exceedingly difficult even in modern settings (Blatt, 1967; Garzanti et al., 2019). Direct petrographic evidence of polycyclic origin is limited to abraded overgrowths and sandstone, siltstone, or shale rock fragments (Johnsson et al., 1988 p.275; Basu, 2017). Only unrobust semiquantitative inferences can thus be drawn. Considering that quartz and ZTR minerals are the most durable detrital components, and therefore the most likely to survive multiple sedimentary cycles, quartz abundance and ZTR-rich depleted tHM suites may be used as indicators of the extent of recycling. It must be kept in mind, however, that even labile grains are recycled in abundance in weathering-limited regime, and that

the effect of selective chemical breakdown attained during diagenesis and inherited during recycling is hardly discriminated from that of intense weathering (Garzanti, 2017).

In South China, quartz abundance is largely controlled by provenance, being markedly more abundant in sand derived from the Cathaysia block than from largely carbonates and basalts of the Yangtze block. Quartz grains with abraded overgrowths are ubiquitous and locally quite common (e.g., Liu catchment), terrigenous rock fragments widespread, and tHM suites invariably poor and mostly very poor, testifying to extensive recycling. Poor tHM suites, however, are also characteristic of detritus shed by low-density – and consequently dense-mineral-poor (Garzanti et al., 2006) – granitic rocks, which are widespread in the Cathaysia block.

As a gross mineralogical indicator of recycling, we may use the Q/F ratio to empirically subdivide the studied samples as follows: A) Q/F ≤ 2, largely first cycle; B) Q/F 2.5-3, partly recycled; C) Q/F 3-4, significantly recycled; D) Q/F 4.5-5.5 extensively recycled ; E) 7-10 mostly recycled; F) 15-20, dominantly recycled. No studied sand displays Q/F < 1.5 or > 20. Group A only includes Nanxi (northern tributary of the Ou River) and Mulanxi sand dominantly derived from granites and felsic volcanic rocks of the SE Coast Magmatic Belt (eastern Cathaysia). Group B includes He, Bei and Xinxing sand derived from the Nanling and Yunkai terranes (western Cathaysia). Group C includes Rong, Gui, Dong, Jiulong, Gan, and mixed Pearl River sand. Group D includes Han and Min sand mainly derived from the Wuyi terrane, as well as Xiang sand to the north and Bazhang sand in Taiwan. Group E includes Hongshui, Yu, and Long sand derived from cover rocks of the Yangtze block as well as Yuan sand to the north and Houlong and Tsengwen sand in Taiwan. Finally, group F includes Beipan, Liu, and Wu sand draining cover rocks of the Yangtze block in the northwestern part of the study area.

5.6. Assessing provenance of Taiwan sandstones

One goal of this study is to establish which specific river system and region of the Chinese mainland originally fed siliciclastic detritus now incorporated in sandstones accreted to the western Taiwan foothills and recycled in modern sand of western Taiwan rivers. Three main possible sources are confronted here: 1) a paleo-Pearl River feeding the South China Sea in the southwest (e.g., figure 9b in Yokoyama et al., 2007); 2) coastal rivers feeding the Taiwan Strait in the west (e.g., Chen et al., 2006; Xu et al., 2014); 3) a paleo-Yangtze River feeding the East China Sea in the north (e.g., figure 9a in Yokoyama et al., 2007; Deng et al., 2017).

A direct comparison with detrital modes of modern sand could have provided a straightforward answer but is precluded because the original mineralogical signature of Taiwan sandstones has undergone significant diagenetic modifications. As a consequence of post-depositional dissolution of unstable minerals, Neogene sandstones of the western Taiwan foothills are notably enriched in durable zircon, tourmaline, rutile, garnet, and apatite (Fig. 5D). This is most clearly shown by sandstones from the TSW core (diagenetic minerofacies 4 of Garzanti et al., 2018, indicating moderate-deep burial). Such a relative enrichment in durable minerals is inherited in modern sands, which display a higher Q/F ratio and more sedimentary rock fragments then their parent sandstones as an effect of progressively increasing detritus recycled from sedimentary rocks of the outer western foothills through time (figure 5 in Nagel et al., 2014). Additional supply of shale and/or carbonate rock fragments from mudrocks and/or carbonates interbedded in source rocks is a common result of physical recycling (Garzanti, 2017).

Because of these reasons, a comparison between Taiwan sandstones and modern sand of the Chinese mainland can be based on the relative proportions of durable minerals only (Fig. 6). Such an approach, similar to what currently done in the correlation of hydrocarbon reservoir sandstones (Morton and Hallsworth, 1994; Morton and McGill, 2018), has large uncertainties but allows us to rule out coastal rivers draining the Wuyi terrane and the SE Coast Magmatic Belt as the dominant source, suggesting that Neogene Taiwan sandstones were fed by a major river system, either a

paleo-Pearl in the south or a paleo-Yangtze in the north. These two potential sources may be discriminated by zircon-age data, although even this method has significant limitations. Age-spectra may be strongly distorted by fertility effects and heavily biased in favour of felsic igneous and metaigneous sources. Moreover, zircon grains recycled even several times from siliciclastic rocks cannot be distinguished from first-cycle grains derived directly from basement rocks.

The comparison of zircon-age data from modern sand of the Zhuoshui and Lanyang Rivers – respectively the largest in western Taiwan and the largest in eastern Taiwan draining exclusively Eocene-Miocene strata of the Hsuehshan and central ranges (Deng et al., 2017) – with datasets from various parts of mainland China, including the Pearl River (He et al., 2019), rivers of SE China (Xu et al., 2007; Xu et al. 2014, 2016), and the Yangtze River (He et al., 2013) provide crucial help. Age spectra in Figure 7 show much greater affinity of Zhuoshui zircons with Yangtze rather than Pearl River zircons, as highlighted further by MDS analysis (Fig. 8). Neogene sandstones of the western Taiwan foothills were thus originally supplied principally by a paleo-Yangtze River.

Yangtze sediments entrained for ~ 1000 km by prevailing southward marine currents (figure 11 in Deng et al., 2017) were deposited on the Chinese passive margin offshore of the present Fujian Province and eventually uplifted and tectonically incorporated in the Taiwan accretionary prism since ~6 Ma (Byrne et al., 2011). As noted by Deng et al. (2017), the zircon signature of Lanyang sand is distinct, reflecting dominant ultimate provenance from the Cathaysia block in pre-Neogene times, thus constraining the timing of the early development of the Yangtze river system (Zheng et al., 2013; Zheng, 2015).

6. Weathering control on sand composition

Tropical to subtropical South China is characterized by a strong climatic gradient, with intensity of annual rainfall that increases steadily from the dry edge of the Tibetan plateau to the humid coastal region heavily hit by the East Asia monsoon (Fig. 3). The different climatic and geomorphologic

conditions in the west and in the east, coupled with notably different source-rock lithologies, account for different weathering regimes, reflected in the distinct mineralogy and geochemistry of sediments generated in the Yangtze and Cathaysia blocks.

6.1. Weathering in the Yangtze block: carbonate grains as weathering tracers

Carbonate strata are widely exposed in western South China and represent a third to more than half of the Wu, Hongshui, Yu, Liu, and Gui catchments (Table 3). None of these rivers, however, carry a corresponding amount of carbonate detritus. Limestone grains, associated with rare dolostone grains in Yu and Beipan sand, represent 15-16% of Hongshui and Yu sand but only 3% of Gui sand, ≤ 1% of Zuo, Long, and Bei sand, and are undetected in Liu and He sand. Downstream, limestone and rare dolostone grains represent only 2-3% of Qian, Xun, and Xi sand and are undetected in Pearl River delta and estuary sand. XRD data on fine silt (<15 μm fraction) reveals the presence of carbonate particles (3-5%) in Beipan, Yu, and Long mud, and geochemical data confirms that carbonate detritus is common in Yu mud and Beipan and You sand, and significant in Beipan and Long mud and in Zuo, Long and Nanpan tributary sand (He et al., companion). In all these catchments, the areal exposure of carbonate rocks far exceeds the percentage of carbonate grains (as quantitatively discussed in subsection 6.4) but two regions are distinguished: 1) a western region drained by the Wu and Hongshui Rivers, where annual rainfall is ~1 m and carbonate grains are preserved although strongly reduced in amount; and, 2) an eastern region drained by the Liu and Gui Rivers, where annual rainfall is ~1.5 m and carbonate grains are rare to negligible. The sharp contrast in the effectiveness of carbonate dissolution in these two regions calls for an explanation that takes into account the peculiarity of geomorphic processes in this wide carbonate domain.

6.2. Karst processes in South China

Thousands of m-thick Devonian to Triassic carbonates exposed in South China are part of one of the world's largest and most spectacular karst terrain (Tang, 2002; Han and Liu, 2004). Two types

of karstic landscapes are identified. *Fengcong* (cone) *karst* (in Chinese *feng*, hill, and *cong*, clustered), dominant in the Yunnan, western Guangxi, and Guizhou Provinces, is characterized by deep dolines and residual conical hills standing on a common base of carbonate bedrock and by mostly underground drainage through a long and deep system of caves. *Fenglin* (tower) *karst* (in Chinese *feng*, hill, and *lin*, isolated), dominant in the eastern Guangxi Province, is an even more advanced form of karst characterized by isolated rock towers rising for 100 m or more from an alluvial plain typically covered by rice paddies. In hot-wet climate with abundant biogenic carbon dioxide and presence of sulfuric acid, bedrock limestone is undercut by dissolution at the water table, promoting gravitational collapse and consequent retreat of vertical cliffs. Fluvial drainage is associated with significant groundwater flow but great caves or large springs do not occur.

In an ideal temporal sequence, tropical karst originating from a peneplaned limestone surface progresses from an intitial stage of doline karst, to *fengcong karst* when dolines enlarge and coalesce to the point of leaving residual conical hills, and next continues to evolve until the doline floor reaches base level. At this point the process changes from surface lowering to lateral planation, thus developing *fenglin karst* (Waltham, 2010).

6.3. Chemical breakdown of carbonate grains in different karst terrains

Karst coverage is estimated to represent 64% of the Hongshui catchment, 42% and 39% of the Yu and Liu catchments, respectively, and as much as 44% of the entire Pearl River basin upstream of the Bei confluence (Li et al., 2016). If in each catchment we compare the percentage of carbonate grains in sand with the extent of karst coverage, then we find ratios between 23% (Hongshui) and 42% (Yu) in terrains characterized by *fengcong karst*. Ratios drop drastically in terrains characterized by *fenglin karst*, where they approach (Gui, Zuo, Long and Bei catchments) or even reach 0% (Liu and He catchments). The same ratios calculated for mud (data from He et al., companion) are consistently lower than for sand, and range 10-15% for the Yu, Beipan and Long Rivers and 0% for the He tributary and Pearl River delta. Carbonate grains are thus reduced to

between less than half and a fifth in sand and to between one sixth and one tenth in mud in terrains characterized by *fengcong karst*, where residual conic hills still share a common base of carbonate bedrock. Instead, they are completely or quasi-completely dissolved in terrains characterized by *fenglin karst*, where tower-like residual rock outcrops are separated by an alluvial plain underlain by a water table containing abundant dissolved carbon dioxide.

In the monsoon-drenched lower reaches of the Pearl River, carbonate sand grains survive in minor amount as far as downstream of the Bei confluence (ratios to carbonate exposures range 5-9% in the Xun to Xi tracts) but were not detected in Pearl River estuary and delta sand and mud, testifying to virtually complete chemical dissolution of carbonate detritus before reaching the South China Sea. In the upper reaches of the Yangtze River, carbonate grains are quite common in all tributaries and in the trunk river as far as the Three Gorges, tend to decrease downstream but are still common at Wuhan, and are preserved as far as the mouth (Vezzoli et al., 2016).

6.4. Sand generation indices as weathering tracers

The sand generation index SGI is defined as the capacity of a given rock unit A to generate sand relative to other rock units (Palomares and Arribas, 1993). Under the assumption of uniform erosion rate across the considered source area, the SGI of rock unit A is dependent only on its mineralogical and textural characteristics and can be calculated as the ratio between its proportional sand contribution S_A/S and its proportional outcrop area A_A/A ($SGI = \frac{S_A}{S}\frac{A}{A_A}$; Vezzoli et al., 2004, 2020). Patterns of variations in SGI indices can be used to investigate how sand-production rates vary for diverse rock types in different climatic and geomorphological settings across southern China. The proportional sand contributions S_A/S for each major rock type in each subcatchment were calculated by reapportioning petrographic and mineralogical data (Table 1) as follows: **carbonate** -> carbonate grains; **basalt** -> mafic volcanic grains and pyroxene; **granite** -> the part of quartz and feldspar grains in proportion 1:2 (considered typical of granitoid rocks) that leaves excess quartz and

feldspar in proportion ~10:1 (considered typical of sandstone); **schist** -> metamorphic grains and metamorphic heavy minerals; **clastics** -> terrigenous rocks fragments, ZTR minerals, excess quartz and feldspar. Felsic volcanic rock fragments were assigned to "basalt" in the Yangtze block and to "granite" in the Cathaysia block. Proportional outcrop areas A_A/A for each subcatchment are from Table 3. Results are displayed in Fig. 10, where the "granite" category comprises schist, and the "clastic" category includes sandstone and mudrock.

Although SGI calculations are approximate, the SGI readily reveals which lithologies are under-represented in detrital assemblages relative to their outcrop area, and which are consequently over-represented. The carbonate SGI highlights the stark contrast between *fengcong karst*, where half of carbonate detritus may survive dissolution, and *fenglin karst*, where carbonate dissolution is virtually complete. The basalt SGI suggests that basaltic detritus survives in drier climate but is prone to be weathered out in humid climate. The granite SGI indicates that feldspar grains persist in drier climate but especially plagioclase starts to be weathered and destroyed as climate becomes wetter and wetter eastwards in the Pearl River catchment or southward along coastal SE China. The SGI, therefore, turned out to be a most useful parameter to highlight the link between climatic gradients and different regimes of sand generation across South China (Fig. 10).

6.5. Weathering in the Cathaysia block: tectosilicates as weathering tracers

Diverse mineralogical and geochemical parameters indicate that weathering conditions become progressively more intense from west to east across South China, associated with higher rainfall fuelled by the East Asia monsoon (Fig. 3). Kaolinite represents an increasing percentage of clay minerals from the headwater to lower course tributaries of the Pearl River, reaching maxium in Dong mud, decreasing progressively with increasing latitude along the coast, and decreasing further away from the coast in southern tributaries of the Yangtze (He et al., companion). Geochemical proxies follow a similar pattern, but are affected far more than clay mineralogy by multiple controls. This is particularly true for sand, where the influence of parent-rock lithology may be

overwhelming (Garzanti and Resentini, 2016). Extracting weathering information from sand composition is therefore challenging (Fig. 11).

Sand carried by rivers of coastal SE China displays clear mineralogical trends. From north to south, quartz increases (r 0.85) at the expense especially of volcanic and other lithic fragments (r - 0.82). The Mic*/F ratio and ZTR minerals also tend to increase (r 0.69 in both cases), whereas the P/F ratio and epidote decrease (r -0.71 and -0.76). The probability that correlation coefficients r > 0.63, > 0.72, and > 0.77 are obtained by chance with 10 data points are less than 5%, 2%, and 1%, respectively (Lee and Lee, 1982), which gives us confidence that these trends are real.

The most durable tectosilicates (i.e., quartz and microcline*) and ZTR minerals tend to increase southward, which suggests that these trends are at least partly controlled by southward increase of rainfall intensity and weathering conditions (Fig. 3). Comparable mineralogical trends from drier western catchments to wetter eastern catchments in the Pearl and Yangtze river basins are, however, less clear. The Q/F ratio does increase but the relative proportions among feldspars are virtually unchanged from He sand in the west to Dong sand in the more humid east. All mineralogical parameters are very similar in sand of the Xiang and Gan tributaries of the Yangtze and in Han sand in the wetter south, which is most readily explained by similar provenance, all three rivers draining the Wuyi terrane of western Cathaysia (Fig. 2).

Mineralogical signatures of sand generated in the Cathaysia block are primarily controlled by different lithologies in different terranes (Fig. 11), namely dominant Yanshanian plutonic and volcanic rocks in eastern Cathaysia and older granitoid rocks in western Cathaysia (Fig. 8). Detrital modes are also strongly influenced by widespread recycling of siliciclastic strata, and discriminating the effect of weathering (chemical dissolution in the present sedimentary cycle) from that of recycling (chemical dissolution during previous cycles of weathering and diagenesis) remains elusive.

6.6. Chemical indices as weathering tracers

The interplaying effects of source-rock lithology, recycling, and weathering may be detangled by integrating mineralogical and geochemical data. In strong weathering conditions, mobile alkali and alkaline-earth metals are expected to behave coherently (i.e., to be all depleted, although to different degrees depending on the durability of hosting minerals), implying positively correlated α^{Al} values all > 1. Inspection of Fig. 12, instead, shows a sharp anticorrelation between two groups of mobile elements. K, Rb and Ba, hosted principally in K-feldspar and muscovite, are undepleted or even enriched relative to the UCC standard in sand largely derived from granites and schists of the Cathaysia block and Jiangnan orogen. Conversely, Ca, Mg, and Sr are undepleted or only scarcely depleted in detritus derived from carbonates and basaltic rocks of the Yangtze block (He et al., companion). This behaviour matches what observed along the pro-side and retro-side of the Taiwan orogen (e.g., figure 10 in Garzanti and Resentini, 2016), indicating that the weathering effect is overwhelmed by the effect of source-rock lithology in sand generated in both southern China and Taiwan. The extent of recycling may be qualitatively evaluated by mineralogical and geochemical proxies (i.e., ZTR index and CIA/WIP ratio; Garzanti et al., 2019) but no mineralogical or geochemical parameter can be considered as a faithful indicator of weathering,

6.7. Heavy minerals as weathering tracers

The degree of corrosion and the percentage of etched grains for each detrital mineral provides direct textural evidence of chemical attack (Andò et al., 2012). Surficial features, however, tell us the state of what is preserved but nothing about how much was destroyed. Downstream of the Pearl River, from the western Hongshui branch to the South China Sea, corrosion indices tend to increase for all minerals (r 0.83, sign. lev. 2%), more clearly for epidote (r 0.89) but erratically for pyroxene and only imperceptlibly for amphibole and garnet. Corroded tourmaline grains first appear in the Xi tract and represent one tenth and a third of total tourmaline grains in deltaic and shelf sand, respectively. A few corroded zircon grains first appear in deltaic sand and represent one fifth of

total zircon grains offshore. In river sand of the SE China coast, corrosion indices are somewhat higher, but do not show any apparent trend from north to south. Similarly, no trend is displayed in sand of southern Yangtze tributaries from west to east.

Pyroxene, one of the least chemically durable minerals at the Earth's surface, is preserved along the course of the Pearl River, where it is progressively diluted downstream by pyroxene-poor sand derived from the western Cathaysia block. The same trend chiefly ascribed to progressive dilution is observed along the Yangtze River, where augite, shed in abundance by the Emeishan Traps in the upper course, persists downstream and represents 5-10% of the tHM suite as far as the mouth. Instead, pyroxene is mostly lacking in rivers of coastal SE China. The only exceptions are the Min River, which carries some corroded to uncorroded augite and minor olivine, and the Beixi tributary of the Jiulong River, which carries mostly uncorroded hypersthene. Although richest in volcanic detritus from the SE Coast Magmatic Belt widely exposed in the Zhejiang province (Fig. 4), Ou sand lacks pyroxene, which suggests complete chemical dissolution. The relative abundance of heavy minerals and their degree of surficial corrosion do provide complementary, but largely qualitative to semiquantitative hints on the intensity of weathering in South China.

7. Conclusion

We have combined petrographic and mineralogical data on sand with the geochemical and clay-mineral data presented in the companion paper (He et al., companion) to study processes of sediment production and dispersal in the wide region of southern China including the Pearl River, the southern tributaries of the Yangtze, and coastal rivers draining the Fujian and Zhejiang Provinces between the two big rivers's mouths.

Southern China can be subdivided into two major geological domains, the Yangtze and Cathyasia blocks. Quartzo-lithic sedimentaclastic sand with augite is shed by the extensive sedimentary and basaltic covers of the Yangtze block, whereas mainly granitic and sedimentary rocks of western

Cathaysia generate feldspatho-quartzose sand including amphibole, epidote, zircon, and tourmaline. Mesozoic magmatic rocks of eastern Cathaysia shed feldspatho-litho-quartzose sand with epidote. The dominance of sedimentary and granitic rocks throughout this vast region is reflected in invariably poor heavy-mineral suites which, together with the occurrence of common terrigenous rock fragments and quartz grains with abraded overgrowths, indicates that sediment generated in southern China is largely polycyclic. An accurate assessment of the amount of first-cycle *versus* recycled detritus, however, remains prohibitive.

Mineralogical signatures in different parts of the Pearl River catchment are sufficiently distinctive to estimate that 35-40% of Pearl River sand is generated from mostly sedimentary and mafic volcanic rocks of the Yangtze block in the western upstream reaches, and 60-65% from mostly felsic igneous and sedimentary rocks of the Cathaysia block in the eastern reaches. Major tributaries supply detritus in subequal proportions, and erosion rates are distributed rather evenly across the drainage basin, reaching ~0.2 mm/a in the Hongshui catchment where topographic relief is greater.

As an attempt to envisage how the present dispersal system operated in the past, we compared petrographic and heavy-mineral data on modern sand and Neogene sandstones, complemented by zircon-geochronology data from the literature, to identify the ultimate sources of siliciclastic detritus originally generated in mainland China and now incorporated in, and recycled from, the Taiwan accretionary prism. It is suggested that sediment supplied by a paleo-Yangtze River was entrained for ~1000 km southward by marine currents and deposited on the Chinese passive margin before being accreted at the front of the Taiwan orogen since ~6 Ma.

A most interesting peculiarity of the western part of the studied region is the extensive exposure of upper Paleozoic to Triassic carbonate rocks, which makes it one of the best known karst areas on Earth. Two types of karstic landscapes are distinguished by the sharply different effectiveness of chemical dissolution. Carbonate grains are attacked by carbonic and sulfuric acids but partly preserved in *fengcong* (cone) *karst*, developed in the Yunnan, Guizhou, and western Guangxi

Provinces, whereas they are completely dissolved in *fenglin* (tower) *karst*, a more advanced form of karst developed in the wetter central-eastern Guangxi Province.

Other factors that can be exploited to trace weathering processes include the different durability of tectosilicates or the degree of surficial corrosion displayed by heavy minerals. These variables do offer useful but largely qualitative to semi-quantitative complementary information, and fail to provide robust proxies for weathering intensity. Although calculations are rough, the sand generation index SGI readily reveals which lithologies are under-represented in detrital assemblages relative to their outcrop area, and which are consequently over-represented. The SGI thus resulted to be a most useful parameter to trace the different regimes of sand generation as closely linked to the strong climatic gradients characterizing South China.

Acknowledgements

We warmly thank Xiangrong Yang and Yunfei Shangguan for fundamental help during sampling, Emanuele Materia for collecting sample #23 offshore of the Pearl River mouth, Giovanni Vezzoli for analysing Pearl River estuary thin sections, and Mara Limonta for supervising heavy-mineral analyses of sand samples from coastal SE China. This study was supported by the National Natural Science Foundation of China (U19B2007, 41702121, 41730531, 41991324), by the State Scholarship Fund from the China Scholarship Council (No. 201906410060), by the Second Tibetan Plateau Scientific Expedition and Research Program (STEP), Ministry of Science and Technology, China (2019QZKK0204), and by MIUR – Dipartimenti di Eccellenza 2018–2022, Department of Earth and Environmental Sciences, University of Milano-Bicocca.

Supplementary Materials

Supplementary data associated with this article, to be found in the online version at http://dx.doi _____, include information on sampling sites (Table A1), petrographic data (Table A2), and heavy-mineral data with frequency of corrosion features (Tables A3 and A4). The Google-Earth™ map of sampling sites PearlProv.kmz is also provided.

FIGURE AND TABLE CAPTIONS

Figure 1. Topography and drainage in tropical and subtropical southern China with sampling sites. PRD: Pearl River Delta.

Figure 2. Tectonic sketch map of southern China (redrawn after the 1:12 000 000 tectonic map of China) with numbered sampling sites. Two blue dashed lines indicate hypothetic boundaries between the Yangtze and Cathaysia blocks (Zhao and Cawood, 2012). **Geological domains**: CF: Chuandian Fragment; ELIP: Emeishan Large Igneous Province; JO: Jiangnan Orogen; QDO: Qinling-Dabie Orogen; SG: Songpan-Ganzi; SWSB: Shiwandashan Structural Belt; YB: Youjiang Basin. **Main faults**: ALF: Anhua-Luocheng, JSF: Jiangshan-Shaoxi; LMF: Longmenshan; RRF: Red River; TLF: Tan-Lu; ZDF: Zhenghe-Dapu. **Taiwan**: CP: Coastal Plain; CR: Central Range; HR: Hsuehshan Range; OR: Coastal Range; WF: Western Foothills.

Figure 3. Rainfall map of SE China (after http://www.chinawater.com.cn) with numbered sampling sites.

Figure 4. Geological map of SE China with sampling sites (after China Geological Map).

Figure 5. Petrography and mineralogy of river sand in southern China and Taiwan. **A**) Array of detrital modes from quartzo-lithic in the Hongshui catchment to feldspatho-quartzose in several coastal rivers of SE China. **B**) Felsic volcanic lithics are dominant in rivers draining the SE Coast Magmatic Belt, whereas sedimentary and mafic volcanic lithics characterize headwater Pearl River tributaries draining the Yangtze block. Metamorphic lithics prevail in sand of Pearl River tributaries draining the Cathaysia block. **C**) The biplot (explanation in subsection 3.3) discriminates three main provenances: a high-ZTR suite recycled from siliciclastic cover strata, a high-clinopyroxene suite

shed from the Emeishan Traps, and a richer amphibole-epidote suite shed from the Cathaysia block. **D**) Array of heavy-mineral modes indicating dominant durable minerals in Miocene to modern Taiwan sediments (data from Ta'an and Tsw cores after Nagel et al., 2014). Q = quartz; F = feldspars; L = lithics (Lm = metamorphic; Lv = volcanic; Ls = sedimentary); tHMC = transparent heavy-mineral concentration: ZTR = zircon + tourmaline + rutile; Grt = garnet; Ap = apatite; Amp = amphibole; Ep = epidote; Px = pyroxene.

Figure 6. Investigating the ultimate provenance of Neogene Taiwan sandstones (biplot explained in subsection 3.3). An excess of recyled sedimentary rock fragments and depleted tHM suites relatively enriched in durable minerals precludes direct comparison with modern sand generated in the Chinese mainland. The comparison of the relative proportions of quartz (Q), K-feldspar (KF), plagioclase (Pl), volcanic lithics (Lv) and durable transparent heavy minerals allows us to discard coastal rivers of SE China and the Cathaysia block as the unique original source. Taiwan sandstones were derived from a larger fluvial system, either the Yangtze in the north or the Pearl River in the south.

Figure 7. U-Pb age spectra of detrital zircon as a complementary means to constrain provenance of Neogene Taiwan sandstones. Early to late Yanshanian (lYe) zircons are dominant in rivers of coastal SE China draining eastern Cathaysia, whereas the three Yanshanian, Indosinian (I) and Wuyi-Yunkai (WY) peaks are the fingerprint of Pearl River sand. Yangtze zircons have much more abundant Jiangnan (J) ages and significant Lüliangian (L) and Wutai-Fuping (WF) clusters reflecting ultimate provenance from the older Yangtze block. Zhuoshui River zircons display all six modes (Yanshanian to Wutai-Fuping) indicating affinity with Yangtze zircons. Lanyang River zircons, instead, display prominent Yanshanian and Wuyi-Yunkai peaks, indicating major contribution from the Cathaysia block in pre-Neogene time (figure 9 in Deng et al., 2017). Sources

of zircon ages: Zhuoshui River and compilations for eastern Cathaysia, western Cathaysia, and Yangtze blocks after Deng et al. (2017); Yangtze River and tributaries after He et al. (2013); Pearl River and tributaries after Xu et al. (2007), Zhao et al. (2015), Liu et al. (2017), Zhong et al. (2017), and He et al. (2019).

Figure 8. MDS map based on U-Pb age spectra of detrital zircon in modern sand (MDS explained in subsection 3.3). The ultimate provenance of multicyclic detritus in western Taiwan is constrained by comparison with data from Pearl River (rhombs for mainstem, triangles for tributaries, names in brown; from Xu et al., 2007, Zhao et al., 2015, Liu et al., 2017, Zhong et al., 2017, and He et al., 2019), rivers in coastal SE China (circles, names in orange; from Xu et al., 2007 and Xu et al., 2014), and Yangtze (stars for mainstem, squares for tributaries, names in blue; from He et al., 2013). Detrital zircons in the Zhuoshui River draining western Taiwan (data from Deng et al., 2017) indicate affinity with Yangtze rather than Pearl River zircons, and minimal affinity with zircons in rivers of coastal SE China.

Figure 9. Areal distribution of *fengcong* and *fenglin karst* (after Waltham, 2010) *versus* carbonate detritus in sand and mud (geochemical and XRD data after He et al., companion). Carbonate grains are drastically depleted but survive in Wu, Hongshui and Yu catchments characterized by *fengcong karst* but are almost completely dissolved in catchments characterized by *fenglin karst.*

Figure 10. Sediment generation indices for carbonate (yellow), basaltic (purple), clastic (grey), and granitic rocks (light blue). In the Yangtze block, the SGI is ≥ 1 for clastics, basalt, and granite (**A**). The carbonate SGI is ~0.5 in *fengcong karst* but goes to 0 in the wetter eastern Guangxi Province characterized by *fenglin karst*, where the clastics SGI consequently increases sharply (**B**). The SGI for basalt, carbonate and granite decreases steadily towards the Pearl River mouth, and the SGI for

clastics consequently increases (**C**). In the Cathaysia block, the granite SGI decreases eastward in the Pearl River catchment (**D**) and increases instead northward in costal rivers (**E**), reflecting trends in weathering intensity controlled by rainfall gradients; the clastics SGI follows a specular path. The SGI remains <0.1 for carbonate, <1 for granite, and >1 for clastics in eastern Yangtze tributaries (**F**).

Figure 11. Modern sand generated in the Cathaysia block (biplot explained in subsection 3.3). Anticorrelation between quartz (Q) and microcline (Mic*), which is the most durable detrital feldspar, and lack of correlation with plagioclase (P) indicate that relative tectosilicate abundance is primarily controlled by provenance (to which the 1st principal component is broadly associated) rather than by weathering and/or recycling (to which the 2nd principal component is broadly associated). Or*: untwinned K-feldspar. ZTR (Hubert, 1962) is a crude indicator of recycling.

Figure 12. Dominant provenance control on detrital modes, tHM suites, and chemical indices (mineralogical parameters as in Fig. 11; biplot and chemical indices explained in subsection 3.3). The α^{Al} values of K, Rb, Ba hosted in K-feldspar and muscovite anticorrelate with α^{Al} values of Ca, Mg, Sr hosted in carbonates, indicating that weathering effects (higher in humid coastal regions of the Cathaysia block) are obscured by the effect of source-rock lithology. Rough mineralogical (ZTR; Hubert, 1962) and chemical (CIA/WIP; Garzanti et al., 2013) indices of recycling are highest in modern sand of western Taiwan.

Table 1. Characteristics of the studied river catchments (data from http://www.chinawater.com.cn, Changjiang Water Resources Commission, 2005; Pearl River Water Resources Commission, 2006; Kao and Milliman, 2008). Sediment yields and erosion rates calculated assuming that bedload is 10% of suspended load and average source-rock density is 2.67 g/cm^3.

Table 2. Key petrographic and heavy-mineral signatures of river sand. Q = quartz; F = feldspars (P = plagioclase; Mic* = cross-hatched microcline); L = lithic grains (Lvm = volcanic to low-rank metavolcanic; Lc = carbonate; Lsm = sedimentary to low-rank metasedimentary; Lm = higher-rank metamorphic); tHMC = transparent heavy-mineral concentration; ZTR = zircon + tourmaline + rutile; Ep = epidote; Grt = garnet; CSKA= chloritoid + staurolite + andalusite + kyanite + sillimanite; Amp = amphibole; Px = pyroxene; &tHM = other transparent heavy minerals. CI = corrosion indices; n.d. = not determined.

Table 3. Distribution of main rock types exposed in different subcatchments of the Pearl and southern Yangtze catchments (areal percentages calculated by the *Getarea.gms* plugin after China Geological Map).

REFERENCES

Andò, S., Garzanti, E., Padoan, M., Limonta, M., 2012. Corrosion of heavy minerals during weathering and diagenesis: a catalog for optical analysis. Sedimentary Geology 280, 165-178.

Basu, A., 2017. Evolution of siliciclastic provenance inquiries: a critical appraisal. In: Mazumder, R. (Ed.), Sediment Provenance, Influences on Compositional Change from Source to Sink. vol. 2. Elsevier, Amsterdam, pp. 5–23. doi.org/10.1016/B978-0-12-803386-9.00002-2 .

Bersani, D., Andò, S., Vignola, P., Moltifiori, G., Marino, I. G., Lottici, P. P., Diella, V., 2009. Micro-Raman spectroscopy as a routine tool for garnet analysis. Spectrochimica Acta Part A: Molecular and Biomolecular Spectroscopy 73(3), 484-491.

Blatt, H., 1967. Provenance determinations and recycling of sediments. Journal of Sedimentary Petrology 37, 1031-1044.

Byrne, T., Chan, Y.C., Rau, R.J., Lu, C.Y., Lee, Y.H. and Wang, Y.J., 2011. The arc–continent collision in Taiwan. In: Brown, D., Ryan, P.D. (eds.), Arc-Continent Collision. Springer, Berlin-Heidelberg, pp. 213-245.

Changjiang Water Resources Commission, 2005. Bulletin of the Changjiang sediment in 2000–2005; http://www.cjw.com.cn (in Chinese).

Chen, C.H., Lu, H.Y., Lin, W., Lee, C.Y., 2006. Thermal event records in SE China coastal areas: constraints from monazite ages of beach sands from two sides of the Taiwan Strait. Chemical Geology 231(1-2), 118-134.

Chen, C.H., Lee, C.Y., Shinjo, R., 2008. Was there Jurassic paleo-Pacific subduction in South China? Constraints from 40Ar/39Ar dating, elemental and Sr–Nd–Pb isotopic geochemistry of the Mesozoic basalts. Lithos 106(1-2), 83-92.

Chen, S.Z., Pei, C.M., 1993. Geology and geochemistry of source rocks of the eastern Pearl River mouth basin, South China Sea. J. Asian Earth Sci. 8, 393–406.

Chen, X.Y., Huang, C.Y., Shao, L., 2018. Characteristics of heavy minerals in modern sediments of Minjiang and Jiulongjiang Rivers, Fujian Province and their provenance implication. Journal of Palaeogeography (Chinese Edition) 20 (04), 637-650 (in Chinese with English abstract).

Comas Cufí, M., Thió Fernández de Henestrosa, S., 2011. CoDaPack 2.0: a stand-alone, multi-platform compositional software.

Dadson, S.J., Hovius, N., Chen, H., Dade,W.B., Hsieh, M.L.,Willett, S.D., Hu, J.C., Horng, M.J., Chen, M.C., Stark, C.P., Lague, D., Lin, J.C., 2003. Links between erosion, runoff variability and seismicity in the Taiwan orogen. Nature 426, 648–651.

Deng, K., Yang, S., Li, C., Su, N., Bi, L., Chang, Y.P., Chang, S.C., 2017. Detrital zircon geochronology of river sands from Taiwan: Implications for sedimentary provenance of Taiwan and its source link with the east China mainland. Earth-Science Reviews 164, 31-47.

Dickinson, W.R., 1985. Interpreting provenance relations from detrital modes of sandstones. In: Zuffa, G.G. (Ed.), Provenance of arenites. Reidel, Dordrecht, NATO ASI Series 148, 333-361.

Dinis, P.A., Garzanti, E., Hahn, A., Vermeesch, P., Cabral-Pinto, M., 2020. Weathering indices as climate proxies. A step forward based on Congo and SW African river muds. Earth-Science Reviews, 201, 103039.

Fujian Institute of Geological Survey, 2015. Regional Geology of Fujian Province. Geological Publishing House, Beijing.

Fuller, C.W., Willett, S.D., Fisher, D., Lu, C.Y., 2006. A thermomechanical wedge model of Taiwan constrained by fission-track thermochronometry. Tectonophysics 425, 1–24.

Gabriel, K.R., 1971. The biplot graphic display of matrices with application to principal component analysis. Biometrika 58, 453–467.

Galehouse, J.S., 1971. Point counting. In: Carver, R.E. (Ed.), Procedures in Sedimentary Petrology. Wiley, New York, pp. 385–407.

Garzanti, E., 2016. From static do dynamic provenance analysis—Sedimentary petrology upgraded, Sediment. Geol. 336, 3–13.

Garzanti, E., 2017. The maturity myth in sedimentology and provenance analysis. Journal of Sedimentary Research 87(4), 353-365.

Garzanti, E., 2019. Petrographic classification of sand and sandstone. Earth-Science Reviews 192 545-563.

Garzanti, E., Andó, S., 2007. Heavy-mineral concentration in modern sands: Implications for provenance interpretation. In: Mange, M.A., Wright, D.T. (Eds.), Heavy Minerals in Use, Developments in Sedimentology Series 58. Elsevier, Amsterdam, pp. 517–545.

Garzanti, E., Andò, S., 2019. Heavy minerals for junior woodchucks. Minerals 9, 148, doi:10.3390/min9030148.

Garzanti, E., Resentini, A., 2016. Provenance control on chemical indices of weathering (Taiwan river sands). Sedimentary Geology 336, 81-95.

Garzanti, E., Vezzoli, G., 2003. A classification of metamorphic grains in sands based on their composition and grade. J. Sediment. Res. 73, 830–837.

Garzanti, E., Vezzoli, G., Ando, S., Castiglioni, G., 2001. Petrology of rifted-margin sand (Red Sea and Gulf of Aden, Yemen). The Journal of Geology 109(3), 277-297.

Garzanti, E., Ando, S., Vezzoli, G., 2006. The continental crust as a source of sand (Southern Alps cross section, northern Italy). The Journal of Geology 114(5), 533-554.

Garzanti, E., Andò, S., Vezzoli, G., 2008. Settling equivalence of detrital minerals and grain-size dependence of sediment composition. Earth and Planetary Science Letters 273(1-2), 138-151.

Garzanti, E., Andò, S., Vezzoli, G., 2009. Grain-size dependence of sediment composition and environmental bias in provenance studies. Earth and Planetary Science Letters 277, 422-432.

Garzanti, E., Vezzoli, G., Andò, S., Lavé, J., Attal, M., France-Lanord, C., DeCelles, P., 2007. Quantifying sand provenance and erosion (Marsyandi River, Nepal himalaya). Earth Planet. Sci. Lett. 258 (3–4), 500–515.

Garzanti, E., Resentini, A., Vezzoli, G., Andò, S., Malusà, M., Padoan, M., 2012. Forward compositional modelling of Alpine orogenic sediments. Sedimentary Geology 280, 149-164.

Garzanti, E., Padoan, M., Andò, S., Resentini, A., Vezzoli, G., Lustrino, M., 2013. Weathering and relative durability of detrital minerals in equatorial climate: Ssand petrology and geochemistry in the East African Rift. The Journal of Geology 121(6), 547-580.

Garzanti, E., Padoan, M., Setti, M., López-Galindo, A., Villa, I.M., 2014. Provenance versus weathering control on the composition of tropical river mud (southern Africa). Chemical Geology 366, 61-74.

Garzanti, E., Andò, S., Limonta, M., Fielding, L., Najman, Y., 2018. Diagenetic control on mineralogical suites in sand, silt, and mud (Cenozoic Nile Delta): Implications for provenance reconstructions. Earth-Science Reviews 185, 122-139.

Garzanti, E., Vermeesch, P., Vezzoli, G., Andò, S., Botti, E., Limonta, M., Dinis, P., Hahn, A., Baudet, D., De Grave, J., Yaya, N.K., 2019. Congo River sand and the equatorial quartz factory. Earth-Science Reviews 197, 102918, doi.org/10.1016/j.earscirev.2019.102918.

Han, G., Liu, C.Q., 2004. Water geochemistry controlled by carbonate dissolution: A study of the river waters draining karst-dominated terrain, Guizhou Province, China. Chemical Geology 204(1-2), 1-21.

He, J., Garzanti, E., Cao, L.C., Wang, H., 2019. The zircon story of the Pearl River (China) from Cretaceous to present. Earth-Science Reviews, 201, 103078, doi.org/10.1016/j.earscirev.2019.103078.

He, J., Garzanti, E., Dinis, P., Yang, S., Wang, H., companion. Provenance versus weathering control on sediment composition in monsoonal subtropical climate (Pearl River and coastal rivers of SE China) - 1. Geochemistry and clay mineralogy. Chemical Geology, in review.

He, M., Zheng, H., Clift, P.D., 2013. Zircon U–Pb geochronology and Hf isotope data from the Yangtze River sands: Implications for major magmatic events and crustal evolution in Central China. Chemical Geology 360, 186-203.

Hovius, N., Stark, C.P., Chu, H.T., Lin, J.C., 2000. Supply and removal of sediment in a landslide dominated mountain belt: Central Range, Taiwan. The Journal of Geology 108, 73–89.

Hu, L., Cawood, P.A., Du, Y., Xu, Y., Xu, W., Huang, H., 2015. Detrital records for Upper Permian-Lower Triassic succession in the Shiwandashan Basin, South China and implication for Permo-Triassic (Indosinian) orogeny. Journal of Asian Earth Sciences 98, 152-166.

Hubert, J.F., 1962. A zircon-tourmaline-rutile maturity index and the interdependence of the composition of heavy mineral assemblages with the gross composition and texture of sandstones. Journal of Sedimentary Research 32 (3), 440–450.

Ingersoll, R.V., 2012. Composition of modern sand and Cretaceous sandstone derived from the Sierra Nevada, California, USA, with implications for Cenozoic and Mesozoic uplift and dissection. Sedimentary Geology 280, 195-207.

Ingersoll, R.V., Bullard, T.F., Ford, R.L., Grimm, J.P., Pickle, J.D., Sares, S.W., 1984. The effect of grain size on detrital modes: a test of the Gazzi-Dickinson point-counting method. Journal of Sedimentary Petrology 54 (1), 103–116.

Jahn, B.M., Zhou, X.H., Li, J.L., 1990. Formation and tectonic evolution of southeastern China and Taiwan: isotopic and geochemical constraints. Tectonophysics 183, 145–160.

Johnsson, M.J., 1993. The system controlling the composition of clastic sediments. In: Johnsson, M.J., and Basu, A. (eds.), Processes Controlling the Composition of Clastic Sediments. Geological Society of America, Special Paper 284, pp. 1-19.

Johnsson, M.J., Stallard, R.F., Meade, R.H., 1988. First-cycle quartz arenites in the Orinoco River basin, Venezuela and Colombia. The Journal of Geology 96, 263–277.

Kao, S.J., Milliman, J.D., 2008. Water and sediment discharge from small mountainous rivers, Taiwan: Tthe roles of lithology, episodic events, and human activities. The Journal of Geology 116, 431-448.

Lee, J.D., Lee, T.D., 1982. Statistics and computer methods in BASIC. Van Nostrand Reinhold, Amsterdam, 198 p.

Li, C., Hu, X.M., Wang, J.G., Vermeesch, P., Garzanti, E., 2020. Sandstone provenance analysis in Longyan supports the existence of a Late Paleozoic continental arc in South China. Tectonophysics 780, doi.org/10.1016/j.tecto.2020.228400.

Li, J., Zhao, G., Johnston, S.T., Dong, S., Zhang, Y., Xin, Y., Wang. W., Sun. H., Yu, Y., 2017. Permo-Triassic structural evolution of the Shiwandashan and Youjiang structural belts, South China. Journal of Structural Geology 100, 24-44.

Li, X.H., 1997. Timing of the Cathaysia Block formation: constraints from SHRIMP U-Pb zircon geochronology. Episodes 20, 188–192.

Li, X.H., 1999. U–Pb zircon ages of granites from the southern margin of the Yangtze Block: timing of Neoproterozoic Jinning: Orogeny in SE China and implications for Rodinia Assembly. Precambrian Research 97(1-2), 43-57.

Li, X.H., Li, W.X., Li, Z.X., Lo, C.H., Wang, J., Ye, M.F., Yang, Y.H., 2009. Amalgamation between the Yangtze and Cathaysia Blocks in South China: constraints from SHRIMP U–Pb

zircon ages, geochemistry and Nd–Hf isotopes of the Shuangxiwu volcanic rocks. Precambrian Res. 174, 117–128.

Li, X.H., Li, Z.X., Li, W.X., 2014. Detrital zircon U–Pb age and Hf isotope constrains on the generation and reworking of Precambrian continental crust in the Cathaysia Block, South China: a synthesis. Gondwana Res. 25 (3), 1202–1215.

Li, Z., Xu, X., Yu, B., Xu, C., Liu, M., Wang, K., 2016. Quantifying the impacts of climate and human activities on water and sediment discharge in a karst region of southwest China. Journal of Hydrology 542, 836-849.

Li, Z.X., Li X.H., 2007. Formation of the 1300-km-wide intracontinental orogen and postorogenic magmatic province in Mesozoic South China: a flat-slab subduction model. Geology 35, 179–182.

Li, Z.X., Li, X.H., Kinny, P.D., Wang, J., Zhang, S., Zhou, H., 2003. Geochronology of Neoproterozoic syn-rift magmatism in the Yangtze Craton, South China and correlations with other continents: evidence for a mantle superplume that broke up Rodinia. Precambrian Research 122(1-4), 85-109.

Li, Z.X., Li, X.H., Wartho, J.A., Clark, C., Li, W.X., Zhang, C.L., Bao, C., 2010. Magmatic and metamorphic events during the early Paleozoic Wuyi- Yunkai orogeny, southeastern South China: New age constraints and pressure-temperature conditions. Geological Society of America Bulletin 122(5-6), 772-793.

Lin, A. T., Watts, A., Hesselbo, S. P., 2003. Cenozoic stratigraphy and subsidence history of the South China Sea margin in the Taiwan region. Basin Research 15(4), 453-478.

Liu, B., Chen, J., Lu, W., Chen, X., Lian, Y., 2016. Spatiotemporal characteristics of precipitation changes in the Pearl River Basin, China. Theoretical and Applied Climatology 123(3-4), 537-550.

Liu, B.J., Xu, X.S., 1994. Paleogeography and Lithofacies Atlas of South China (Sinian–Triassic). The Series of Paleogeography and Lithofacies of South China. Science Press, Beijing, 192 p. (in Chinese).

Liu, C., Clift, P.D., Carter, A., Böning, P., Hu, Z., Sun, Z., Pahnke, K., 2017. Controls on modern erosion and the development of the Pearl River drainage in the late Paleogene. Marine Geology 394, 52–68

Liu, Z., Tuo, S., Colin, C., Liu, J.T., Huang, C.-Y., Selvaraj, K., Chen, C.T.A., Zhao, Y., Siringan, F.P., Boulay, S., Chen, Z., 2008. Detrital fine-grained sediment contribution from Taiwan to the northern South China Sea and its relation to regional ocean circulation. Marine Geology 255, 149–155

Ma, X. H., Han, Z.Z., Bi, S.P., Hu, G., Zhang, Y., Xu, C.F., 2018. Heavy mineral composition in surface sediments of the Minjiang River estuary and its implication for provenance. Marine Geology & Quaternary Geology 38 (01), 87-95 (in Chinese with English abstract).

Milliman, J.D., Farnsworth, K.L., 2013. River discharge to the coastal ocean: a global synthesis. Cambridge University Press, Cambridge, NY., 383 p.

Montgomery, D.R., Huang, M.Y.F., Huang, A.Y.L., 2014. Regional soil erosion in response to land use and increased typhoon frequency and intensity, Taiwan. Quaternary Research 81, 15–20.

Morton, A.C., Hallsworth, C., 1994. Identifying provenance-specific features of detrital heavy mineral assemblages in sandstones. Sedimentary Geology 90(3-4), 241-256.

Morton, A.C., McGill, P., 2018. Correlation of hydrocarbon reservoir sandstones using heavy mineral provenance signatures: Examples from the North Sea and adjacent areas. Minerals 8, 564, doi:10.3390/min8120564.

Nagel, S., Castelltort, S., Wetzel, A., Willett, S.D., Mouthereau, F., Lin, A.T., 2013. Sedimentology and foreland basin paleogeography during Taiwan arc continent collision. Journal of Asian Earth Sciences 62, 180–204.

Nagel, S., Castelltort, S., Garzanti, E., Lin, A. T., Willett, S. D., Mouthereau, F., Limonta, M., Adatte, T., 2014. Provenance evolution during arc–continent collision: sedimentary petrography of Miocene to Pleistocene sediments in the western foreland basin of Taiwan. Journal of Sedimentary Research 84(7), 513-528.

Nesbitt, H.W., Young, G.M., 1982. Early Proterozoic climates and plate motions inferred from major element chemistry of lutites. Nature 299, 715–717.

Nesbitt, H.W., Fedo, C.M., Young, G.M., 1997. Quartz and feldspar stability, steady and non-steady-state weathering, and petrogenesis of siliciclastic sands and muds. The Journal of Geology 105(2), 173-192.

Ottens, B., Cook, R.B., 2005. The Yaogangxian Tungsten Mine. Rocks & Minerals 80(1), 46-57.

Palomares, M., Arribas, J., 1993. Modern stream sands from compound crystalline sources: Composition and sand generation index. In: Johnsson, M.J., Basu, A, (eds.), Processes controlling the composition of clastic sediments. Geological Society of America, Special Paper 284, 313-322.

Parker, A., 1970. An index of weathering for silicate rocks. Geologival Magazine 107. 501–504.

Pearl River Water Resources Commission, 2006. http://www.pearlwater.gov.cn (in Chinese).

Qiu, Y.M., Gao, S., McNaughton, N.J., Groves, D.I., Ling, W., 2000. First evidence of > 3.2 Ga continental crust in the Yangtze craton of south China and its implications for Archean crustal evolution and Phanerozoic tectonics. Geology 28(1), 11-14.

Resentini, A., Goren, L., Castelltort, S., Garzanti, E., 2017. Partitioning the sediment flux by provenance and tracing erosion patterns in Taiwan. Journal Geophysical Research - Earth Surface, 122, doi:10.1002/2016JF004026.

Rudnick, R.L., Gao, S., 2003. Composition of the continental crust. In: Rudnick, R.L., Holland, H.D., Turekian, K.K. (Eds.), Treatise on Geochemistry. The Crust, 3. Elsevier Pergamon, Oxford, pp. 1–64.

Shellnutt, J.G., 2014. The Emeishan large igneous province: a synthesis. Geosci. Front. 5, 369–394.

Shu, L.S., 2006. Pre-Devonian tectonic evolution of South China: From Cathaysian block to Caledonian folded orogenic belt. Geol. J. China Univ. 12, 418–431.

Shu, L.S., Faure, M., Yu, J.H., Jahn, B.M., 2011. Geochronological and geochemical features of the Cathaysia block (South China): new evidence for the Neoproterozoic breakup of Rodinia. Precambrian Res. 187, 263–276.

Song, X.Y., Zhou, M.F., Hou, Z.Q., Cao, Z.M., Wang, Y.L., Li, Y., 2001. Geochemical constraints on the mantle source of the upper Permian Emeishan continental flood basalts, southwestern China. International Geology Review 43(3), 213-225.

Tang, T., 2002. Surface sediment characteristics and tower karst dissolution, Guilin, southern China. Geomorphology 49(3-4), 231-254.

Taylor, S.R., McLennan, S.M., 1995. The geochemical evolution of the continental crust. Rev. Geophys. 33, 241–265.

Tong, W.X., Tobisch, O.T., 1996. Deformation of granitoid plutons in the Dongshan area, southeast China: constraints on the physical conditions and timing of movement along the Changle-Nanao shear zone. Tectonophysics 267(1-4), 303-316.

Vermeesch, P., 2013. Multi-sample comparison of detrital age distributions. Chemical Geology 341, 140-146.

Vermeesch, P., 2018. Dissimilarity measures in detrital geochronology, Earth-Science Reviews 178, 310-321.

Vermeesch, P., Garzanti, E., 2015. Making geological sense of 'Big Data' in sedimentary provenance analysis. Chemical Geology 409, 20-27.

Vermeesch, P., Resentini, A., Garzanti, E., 2016. An R package for statistical provenance analysis. Sedimentary Geology 336, 14-25.

Vezzoli, G., Garzanti, E., Monguzzi, S., 2004. Erosion in the western Alps (Dora Baltea basin): 1. Quantifying sediment provenance. Sedimentary Geology 171(1-4), 227-246.

Vezzoli, G., Garzanti, E., Limonta, M., Andò, S., Yang, S., 2016. Erosion patterns in the Changjiang (Yangtze River) catchment revealed by bulk-sample versus single-mineral provenance budgets. Geomorphology 261, 177-192.

Vezzoli, G., Garzanti, E., Limonta, M., Radeff, G., 2020. Focused erosion at the core of the Greater Caucasus: Sediment generation and dispersal from Mt. Elbrus to the Caspian Sea. Earth-Science Reviews 200, 102987, doi.org/10.1016/j.earscirev.2019.102987.

von Eynatten, H., Tolosana-Delgado, R., Karius, V., Bachmann, K., Caracciolo, L., 2016. Sediment generation in humid Mediterranean setting: Grain-size and source-rock control on sediment geochemistry and mineralogy (Sila Massif, Calabria). Sedimentary Geology 336, 68-80.

Waltham, T., 2010. Guangxi karst: The fenglin and fengcong karst of Guilin and Yangshuo. In: Migon, P. (ed.), Geomorphological Landscapes of the World. Springer, Dordrecht, pp. 293-302.

Wan, Y., Liu, D., Xu, M., Zhuang, J., Song, B., Shi, Y., Du, L., 2007. SHRIMP U–Pb zircon geochronology and geochemistry of metavolcanic and metasedimentary rocks in Northwestern Fujian, Cathaysia block, China: Tectonic implications and the need to redefine lithostratigraphic units. Gondwana Res. 12, 166–183.

Wang, D., Shu, L., 2012. Late Mesozoic basin and range tectonics and related magmatism in Southeast China. Geoscience Frontiers 3(2), 109-124.

Wang, D., Zheng, J., Ma, Q., Griffin, W.L., Zhao, H., Wong, J., 2013. Early Paleozoic crustal anatexis in the intraplate Wuyi–Yunkai orogen, South China. Lithos 175, 124-145.

Wang, L.J., Yu, J.H., Griffin, W.L., O'Reilly, S.Y., 2012. Early crustal evolution in the western Yangtze Block: Evidence from U–Pb and Lu–Hf isotopes on detrital zircons from sedimentary rocks. Precambrian Research 222, 368-385.

Wang, X.L., Zhou, J.C., Griffin, W.A., Wang, R.C., Qiu, J.S., O'Reilly, S.Y., Xu, X., Liu, X.M., Zhang, G.L., 2007. Detrital zircon geochronology of Precambrian basement sequences in the Jiangnan orogen: Dating the assembly of the Yangtze and Cathaysia Blocks. Precambrian Research 159(1-2), 117-131.

Wang, X.L., Zhou, J.C., Griffin, W.L., Zhao, G., Yu, J.H., Qiu, J.S., Zhang. Y.J., Xing, G.F., 2014. Geochemical zonation across a Neoproterozoic orogenic belt: isotopic evidence from granitoids and metasedimentary rocks of the Jiangnan orogen, China. Precambrian Research 242, 154-171.

Weltje, G.J., von Eynatten, H., 2004. Quantitative provenance analysis of sediments: Review and outlook. Sedimentary Geology 171(1-4), 1-11.

Xia, Y., Xu, X.S., Zhu, K.Y., 2012. Paleoproterozoic S- and A-type granites in southwestern Zhejiang: Magmatism, metamorphism and implications for the crustal evolution of the Cathaysia basement. Precambrian Research 216–219, 177–207.

Xiang, H., Shao, L., Qiao, P., Zhao, M., 2011. Characteristics of heavy minerals in Pearl River sediments and their implications for provenance. Marine Geology & Quaternary Geology 31 (6), 27-35 (in Chinese with English abstract).

Xu, M.Q., Li, C., 2003. Characteristics of heavy minerals composition and distribution in sediment from Jiulong River estuary. Marine Science Bulletin 4, 32-40 (in Chinese with English abstract).

Xu, X., O'Reilly, S.Y., Griffin, W.L., Wang, X., Pearson, N.J., He, Z., 2007. The crust of Cathaysia: age, assembly and reworking of two terranes. Precambrian Res. 158, 51–78.

Xu, Y., Sun, Q., Yi, L., Yin, X., Wang, A., Li, Y., Chen, J., 2014. Detrital zircons U-Pb age and Hf isotope from the western side of the Taiwan Strait: Implications for sediment provenance and crustal evolution of the northeast Cathaysia block. Terrestrial, Atmospheric & Oceanic Sciences, 25(4), 505-535.

Xu, Y., Wang, C.Y., Zhao, T., 2016. Using detrital zircons from river sands to constrain major tectono-thermal events of the Cathaysia Block, SE China. Journal of Asian Earth Sciences 124, 1-13.

Yang, J., Cawood, P.A., Du, Y., Huang, H., Hu, L., 2012. Detrital record of Indosinian mountain building in SW China: Provenance of the Middle Triassic turbidites in the Youjiang Basin. Tectonophysics 574, 105-117.

Yao, J., Shu, L., Cawood, P.A., Li, J., 2016. Delineating and characterizing the boundary of the Cathaysia Block and the Jiangnan orogenic belt in South China. Precambrian Research 275, 265-277.

Yokoyama, K., Tsutsumi, Y., Lee, C.S., Shen, J.J.S., Lan, C.Y., Zhao, L., 2007. Provenance study of tertiary sandstones from the Western foothills and Hsuehshan Range, Taiwan. Bulletin of the National Museum of Nature and Science, Serial C 33, 7-26.

Yu, J.H., O'Reilly, S.Y., Zhao, L., Griffin, W.L., Zhang, M., Zhou, X., Jiang, S.Y., Wang, L.J., Wang, R.C., 2007. Origin and evolution of topaz-bearing granites from the Nanling Range, South China: A geochemical and Sr–Nd–Hf isotopic study. Mineralogy and Petrology 90(3-4), 271-300.

Yu, J.H., Wang, L., O'reilly, S., Griffin, W., Zhang, M., Li, C., Shu, L., 2009. A Paleoproterozoic orogeny recorded in a long-lived cratonic remnant (Wuyishan terrane), eastern Cathaysia Block, China. Precambrian Res. 174, 347–363.

Yu, J.H., O'Reilly, S.Y., Wang, L., Griffin, W.L., Zhou, M.-F., Zhang, M., Shu, L., 2010. Components and episodic growth of Precambrian crust in the Cathaysia Block, South China: evidence from U–Pb ages and Hf isotopes of zircons in Neoproterozoic sediments. Precambrian Res. 181, 97–114.

Zhang, Q., Xiao, M., Singh, V.P., Li, J., 2012. Regionalization and spatial changing properties of droughts across the Pearl River basin, China. J. Hydrol. 472-473, 355–366.

Zhao, G., 2015. Jiangnan Orogen in South China: Developing from divergent double subduction. Gondwana Research 27(3), 1173-1180.

Zhao, G., Cawood, P.A., 2012. Precambrian geology of China. Precambrian Res. 222, 13–54.

Zhao, M., Shao, L., Qiao, P., 2015. Characteristics of Detrital Zircon U-Pb geochronology of the Pearl River Sands and its implication on provenances. Journal Tongji University Natural Sciences 43, 89–97 (in Chinese with English abstract).

Zheng, H., 2015. Birth of the Yangtze River: age and tectonic-geomorphic implications. National Science Review 2(4), 438-453.

Zheng, H., Clift, P.D., Wang, P., Tada, R., Jia, J., He, M., Jourdan, F., 2013. Pre-Miocene birth of the Yangtze River. Proceedings of the National Academy of Sciences 110(19), 7556-7561.

Zhong, L., Li, G., Yan, W., Xia, B., Feng, Y., Miao, L. and Zhao, J., 2017. Using zircon U–Pb ages to constrain the provenance and transport of heavy minerals within the northwestern shelf of the South China Sea. Journal of Asian Earth Sciences 134, 176-190.

Zhou, X.M., Sun, T., Shen, W.Z., Shu, L.S., Niu, Y.L., 2006. Petrogenesis of Mesozoic granitoids and volcanic rocks in South China: a response to tectonic evolution. Episodes 29 (1), 26–33.

Figure 1

Click here to download high resolution image

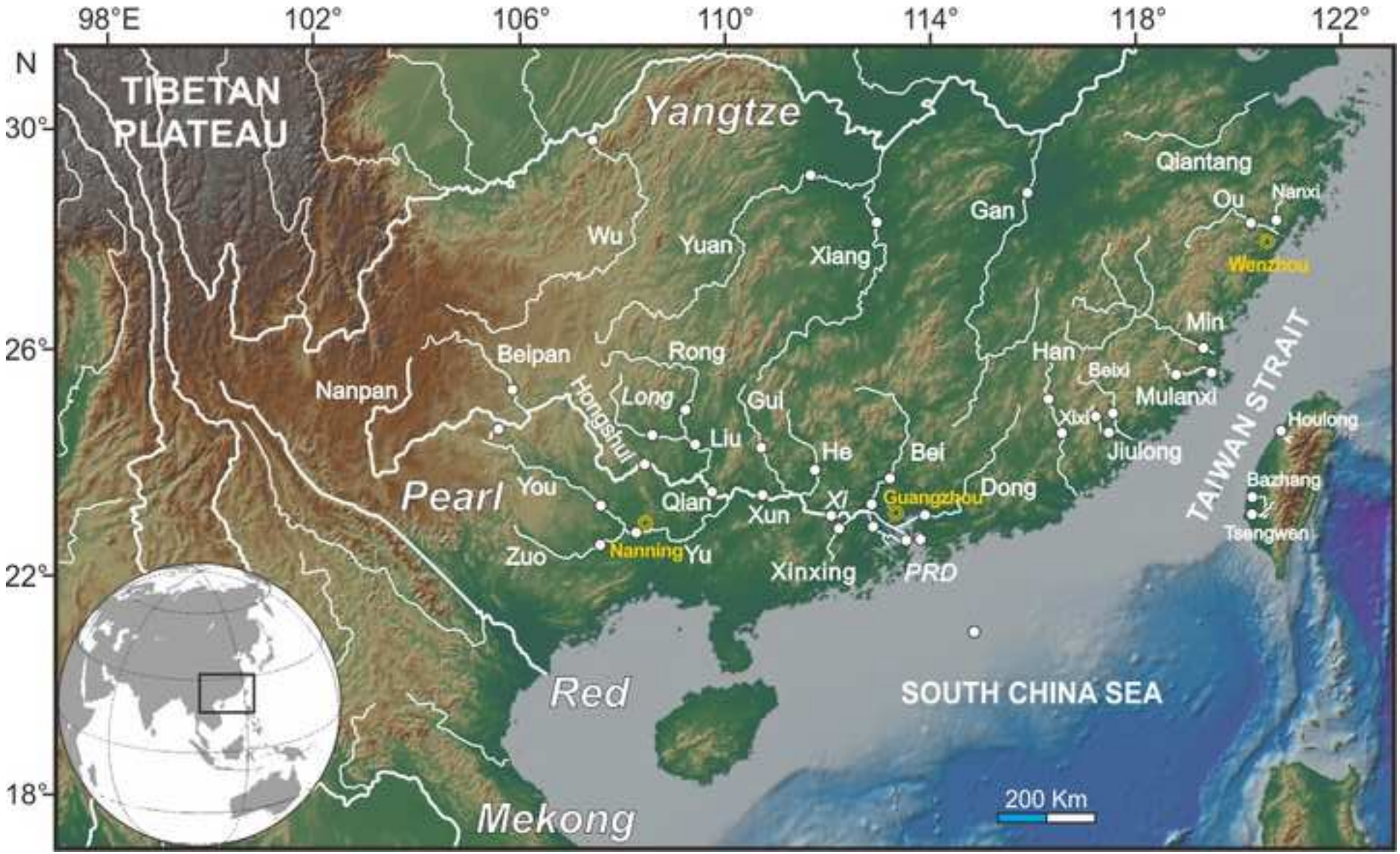

Figure 2

Click here to download high resolution image

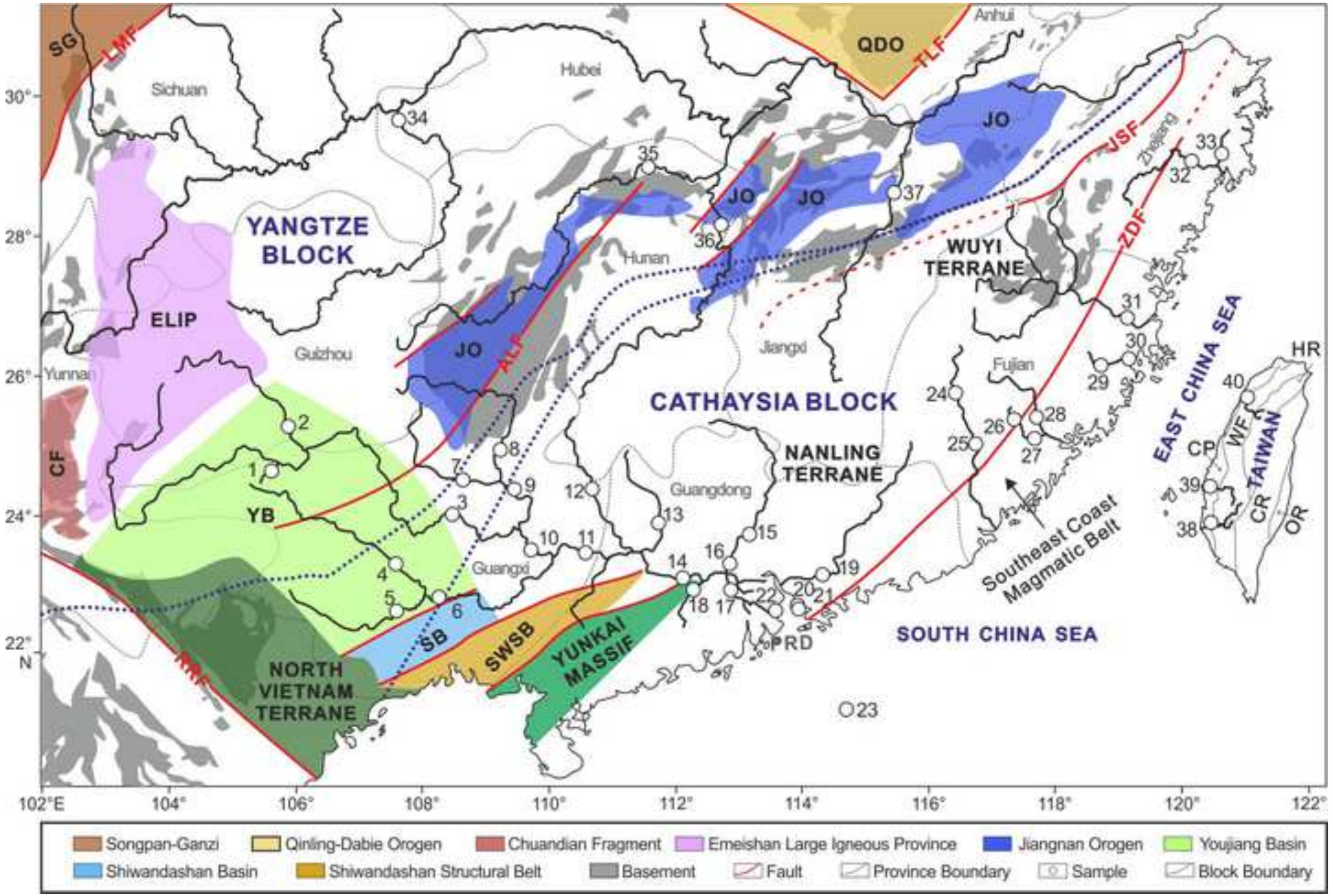

Figure 3

Click here to download high resolution image

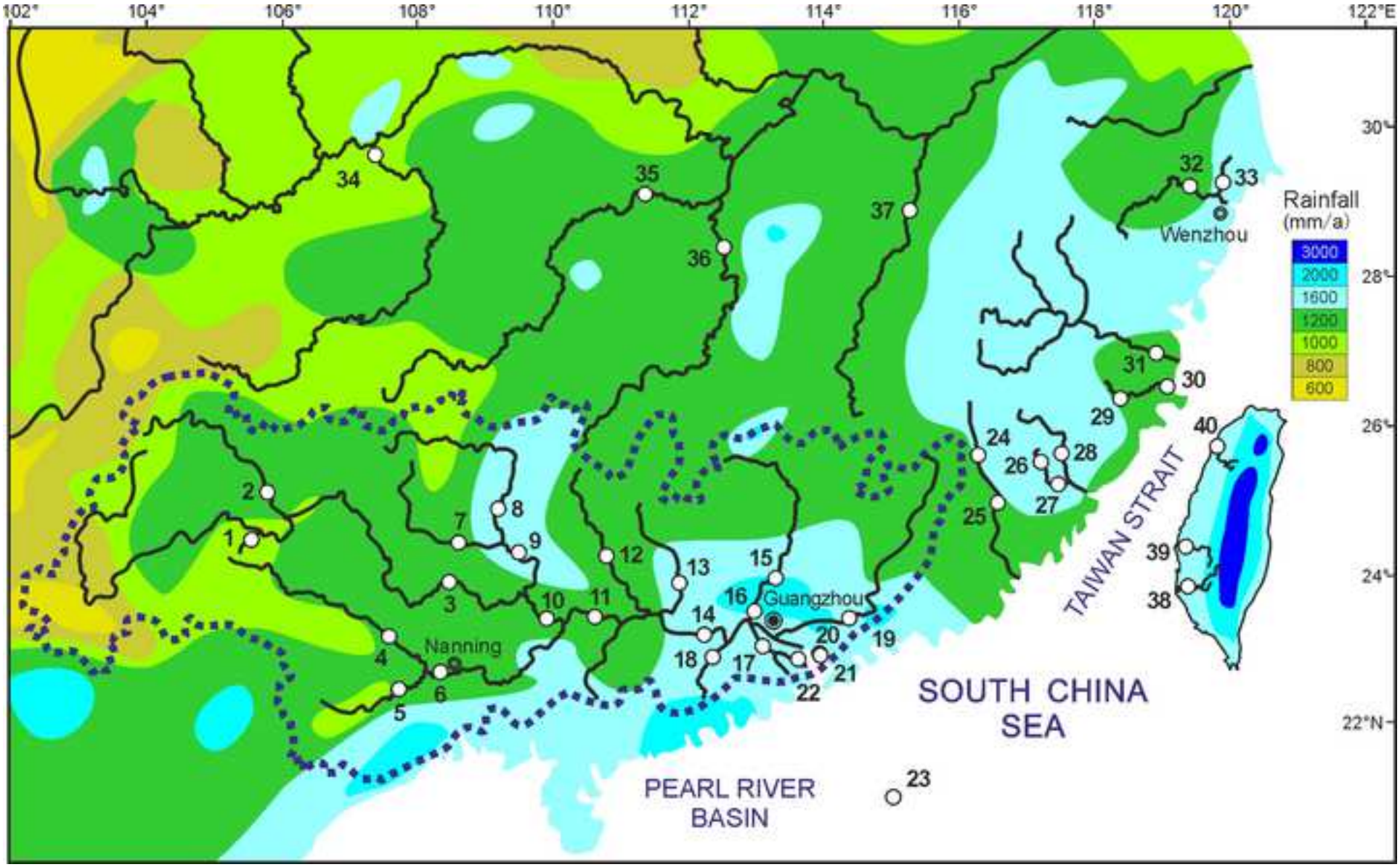

Figure 4

Click here to download high resolution image

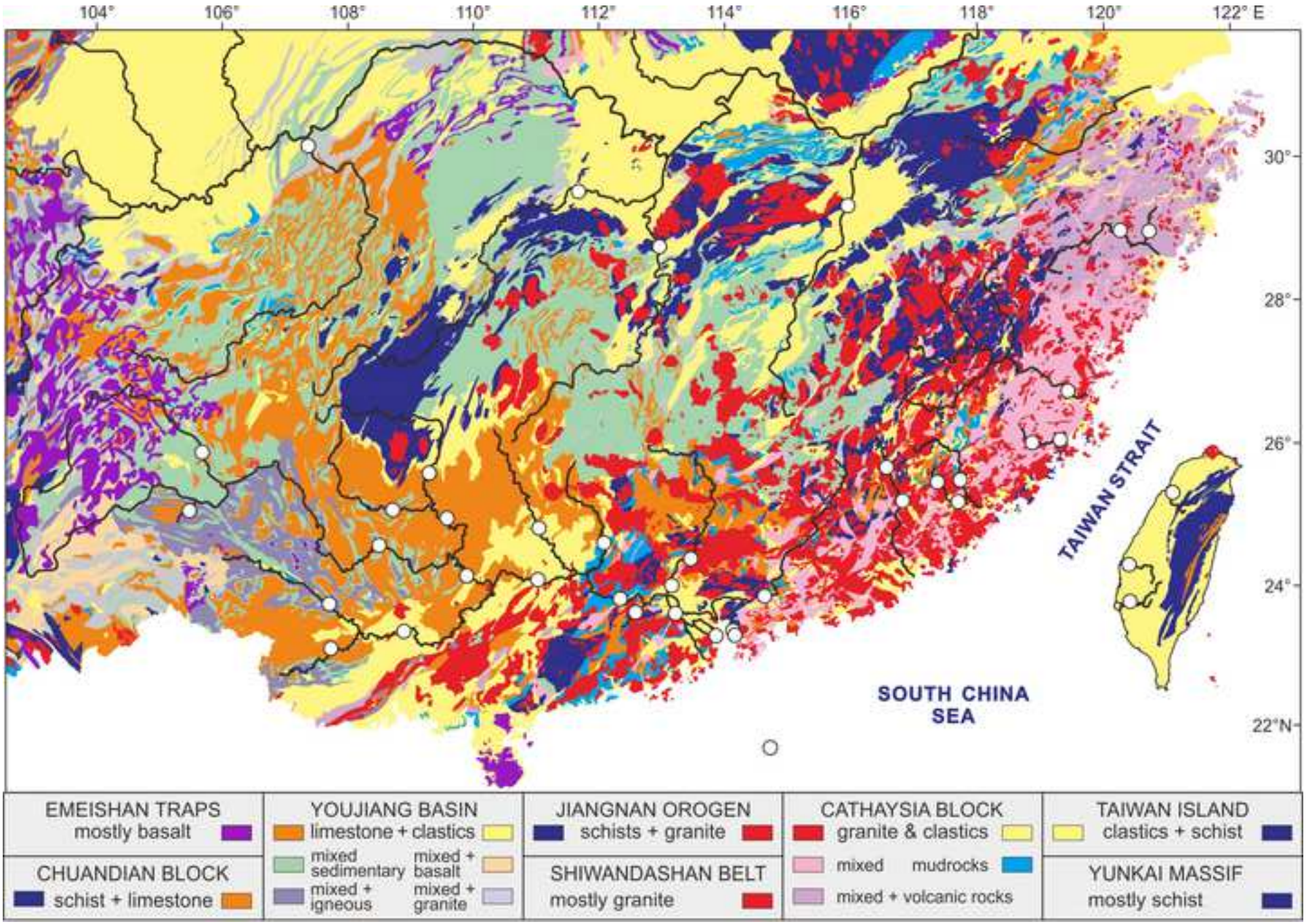

Figure 5

Click here to download high resolution image

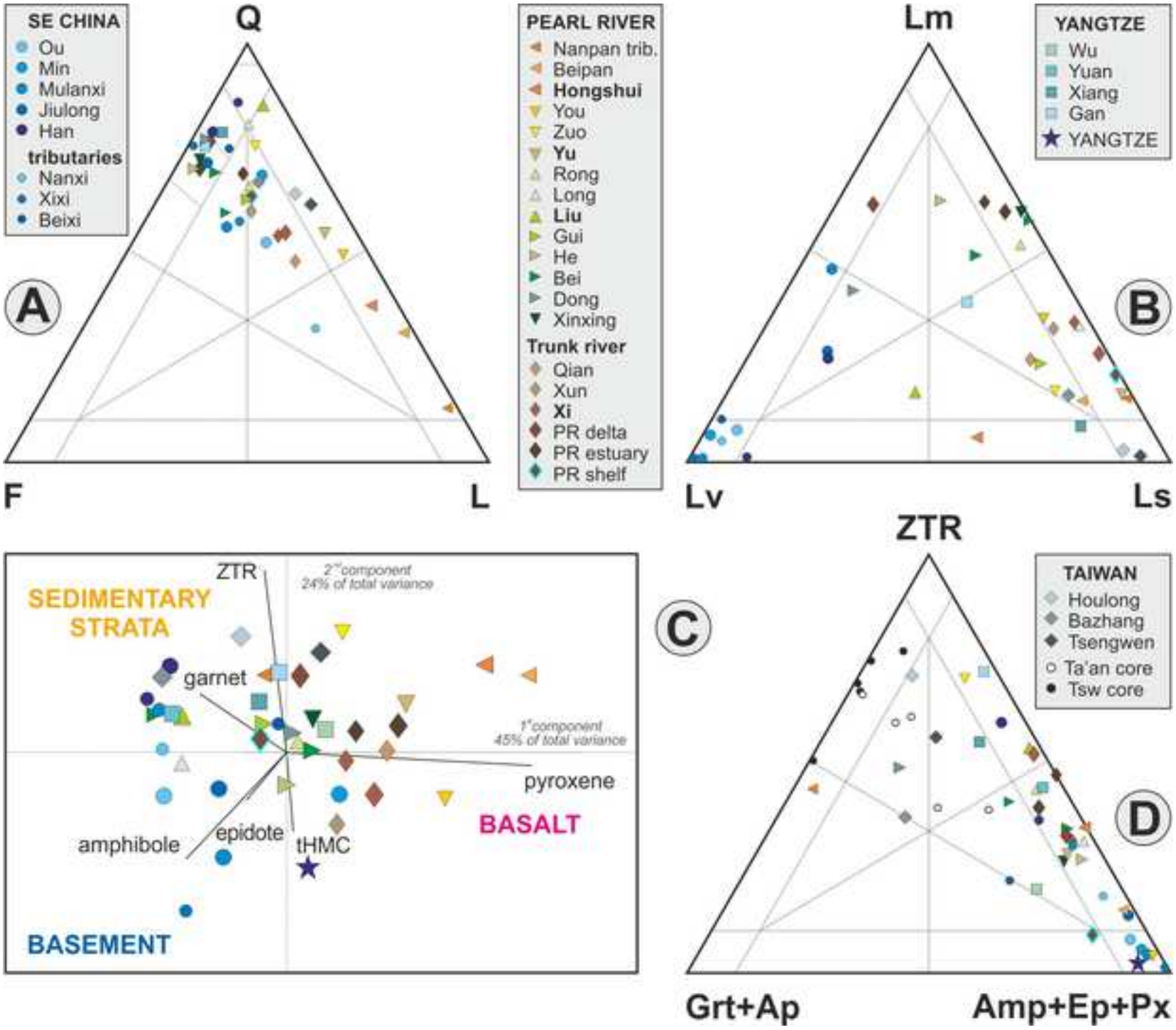

Figure 6

Click here to download high resolution image

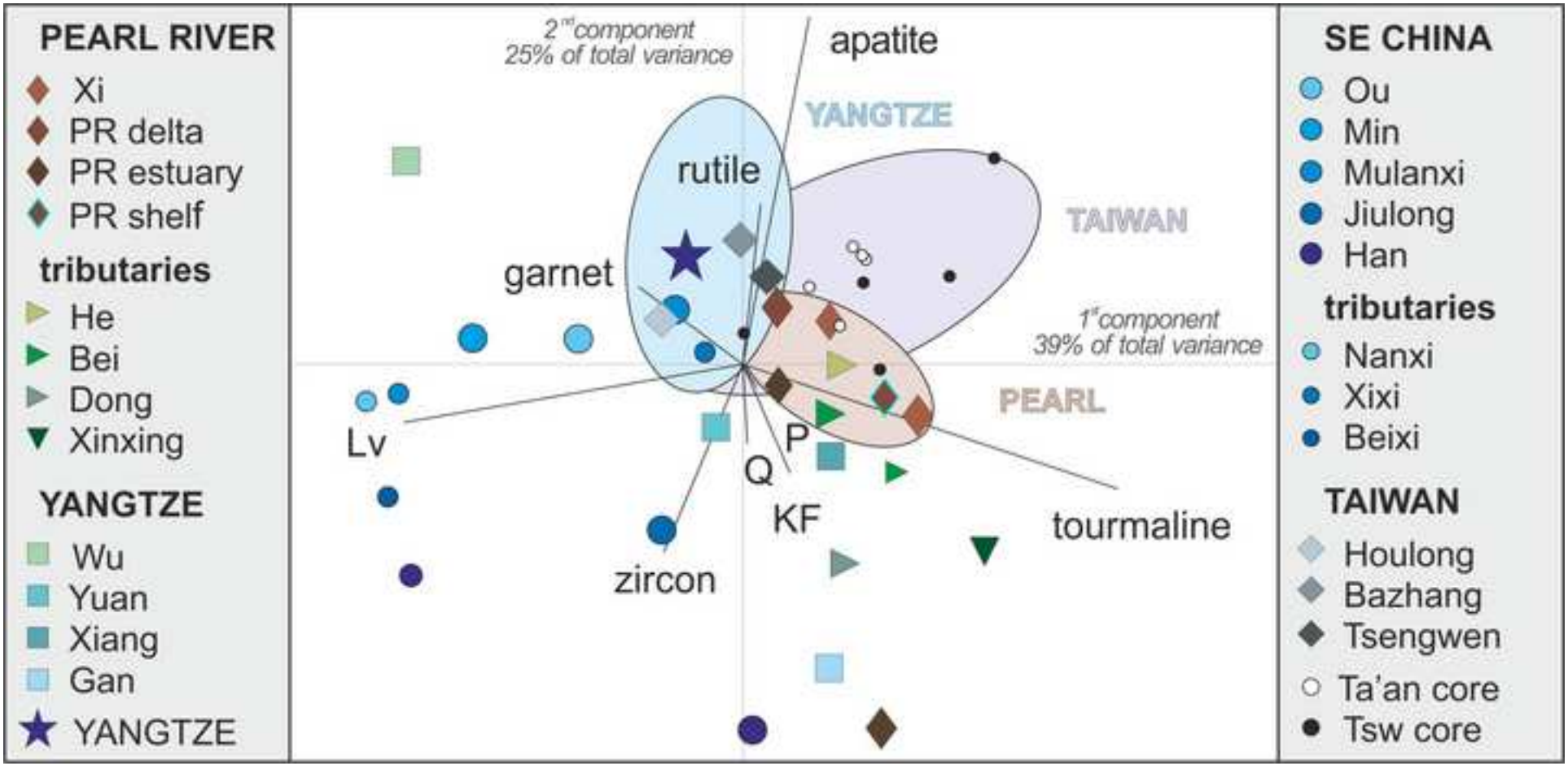

Figure 7

Click here to download high resolution image

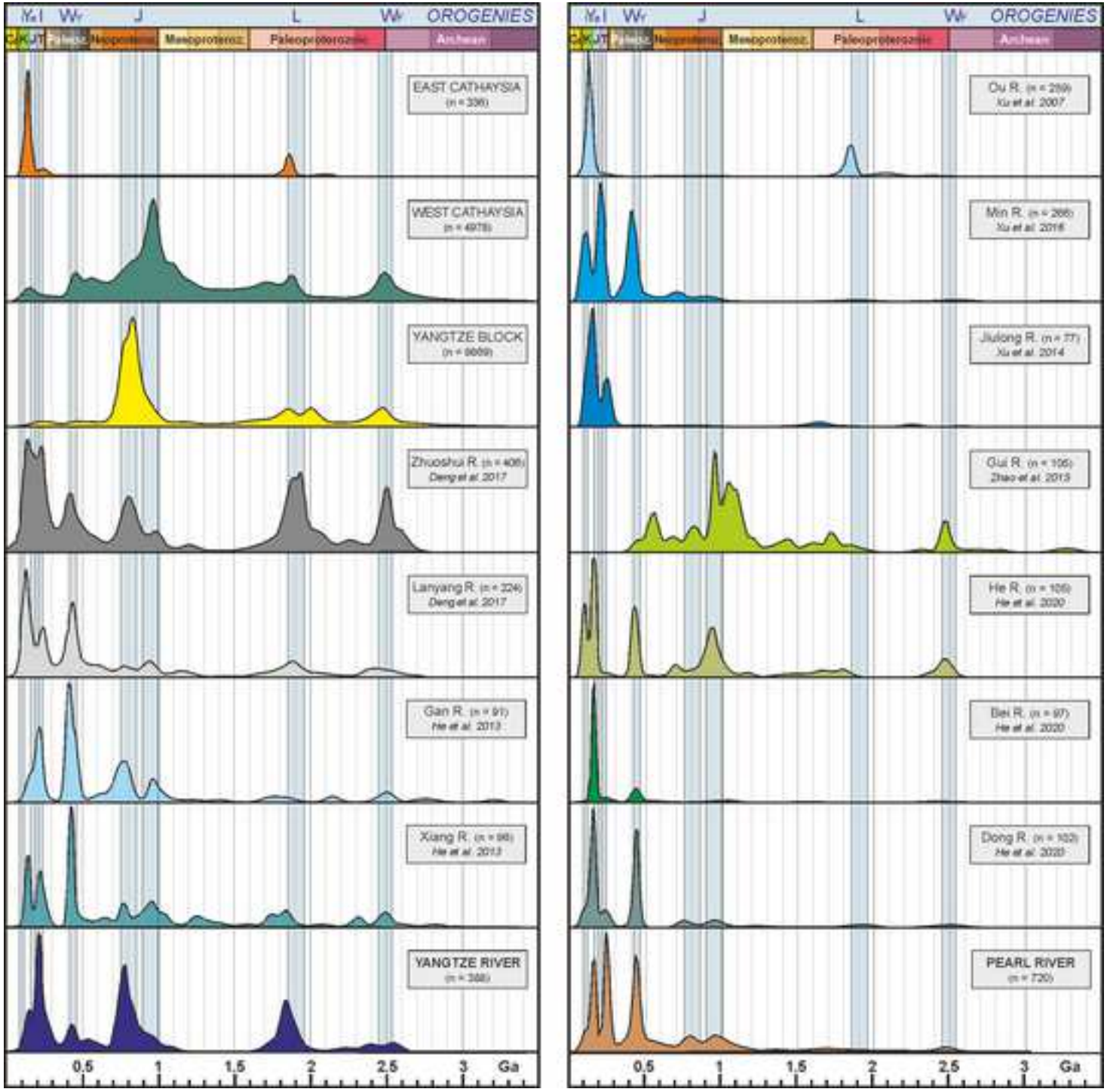

Figure 8

Click here to download high resolution image

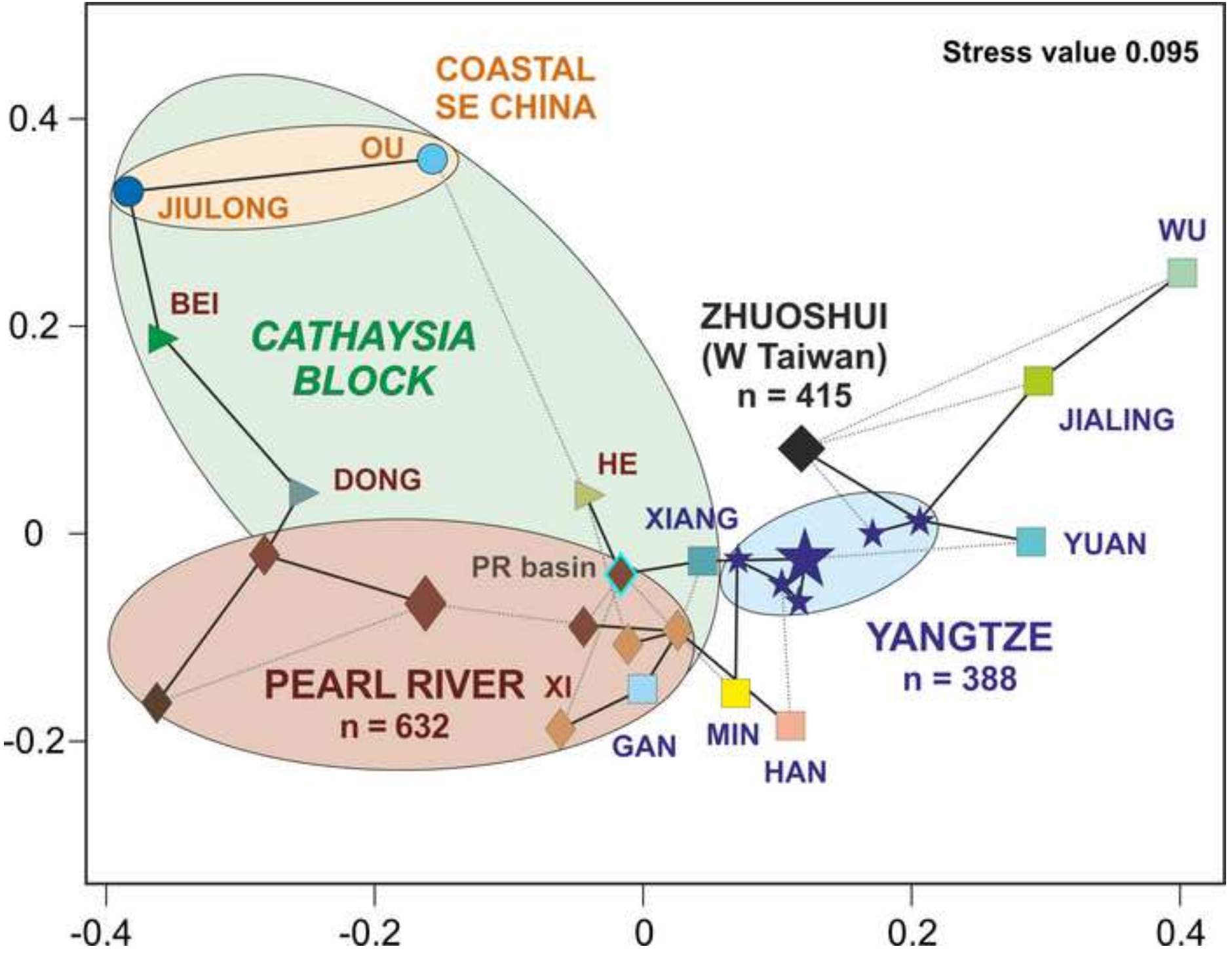

Figure 9

Click here to download high resolution image

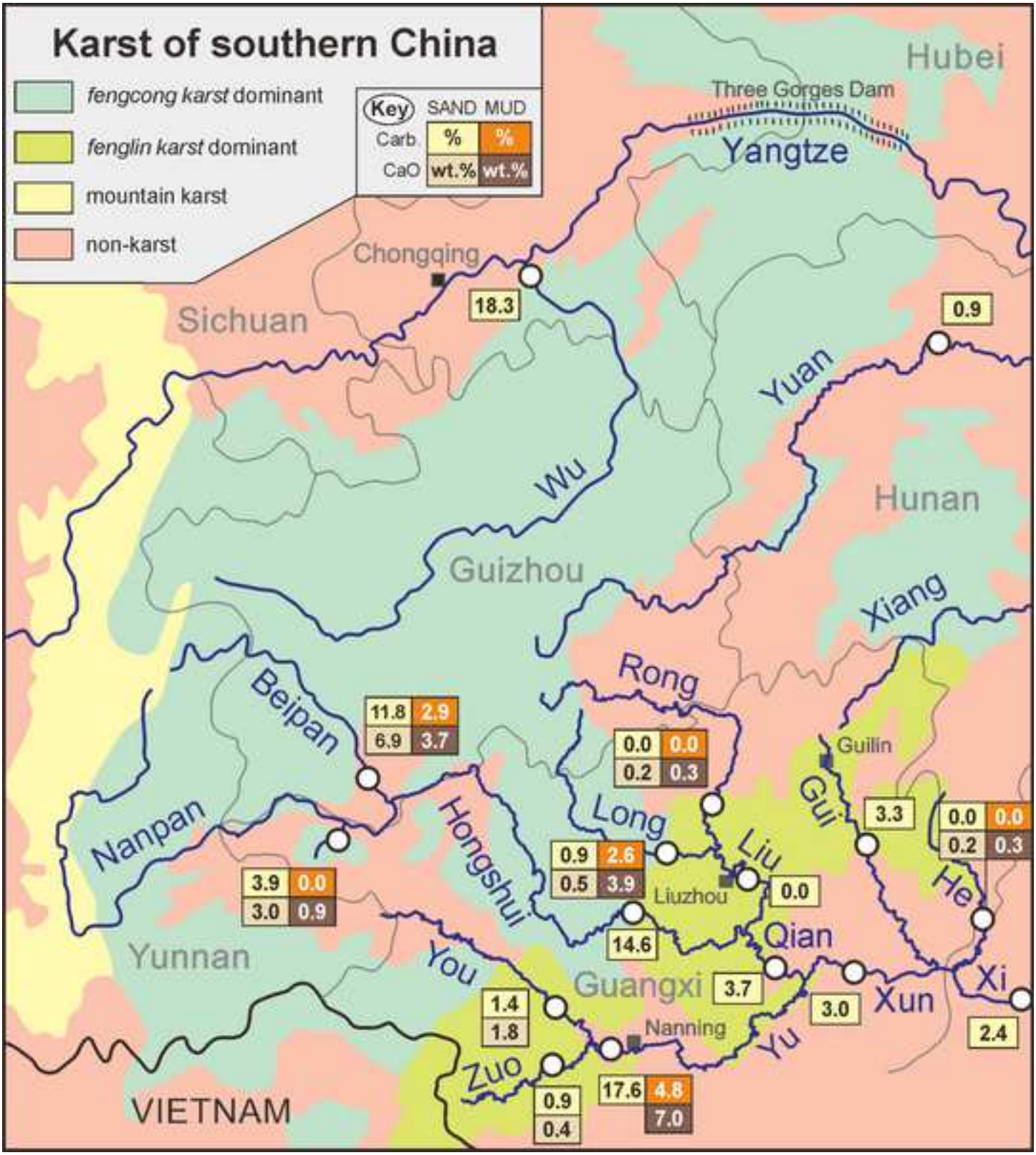

Figure 10

Click here to download high resolution image

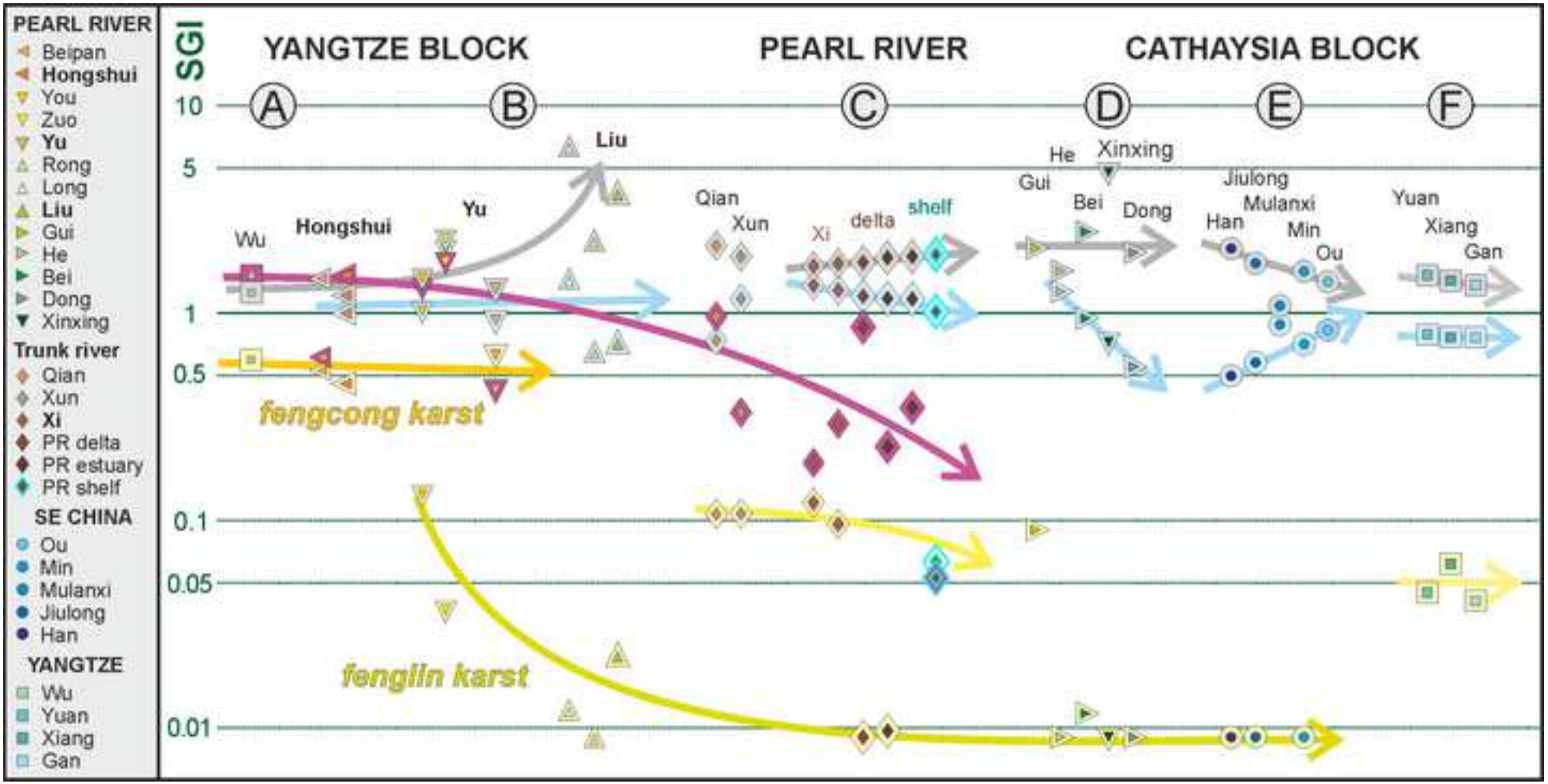

Figure 11

Click here to download high resolution image

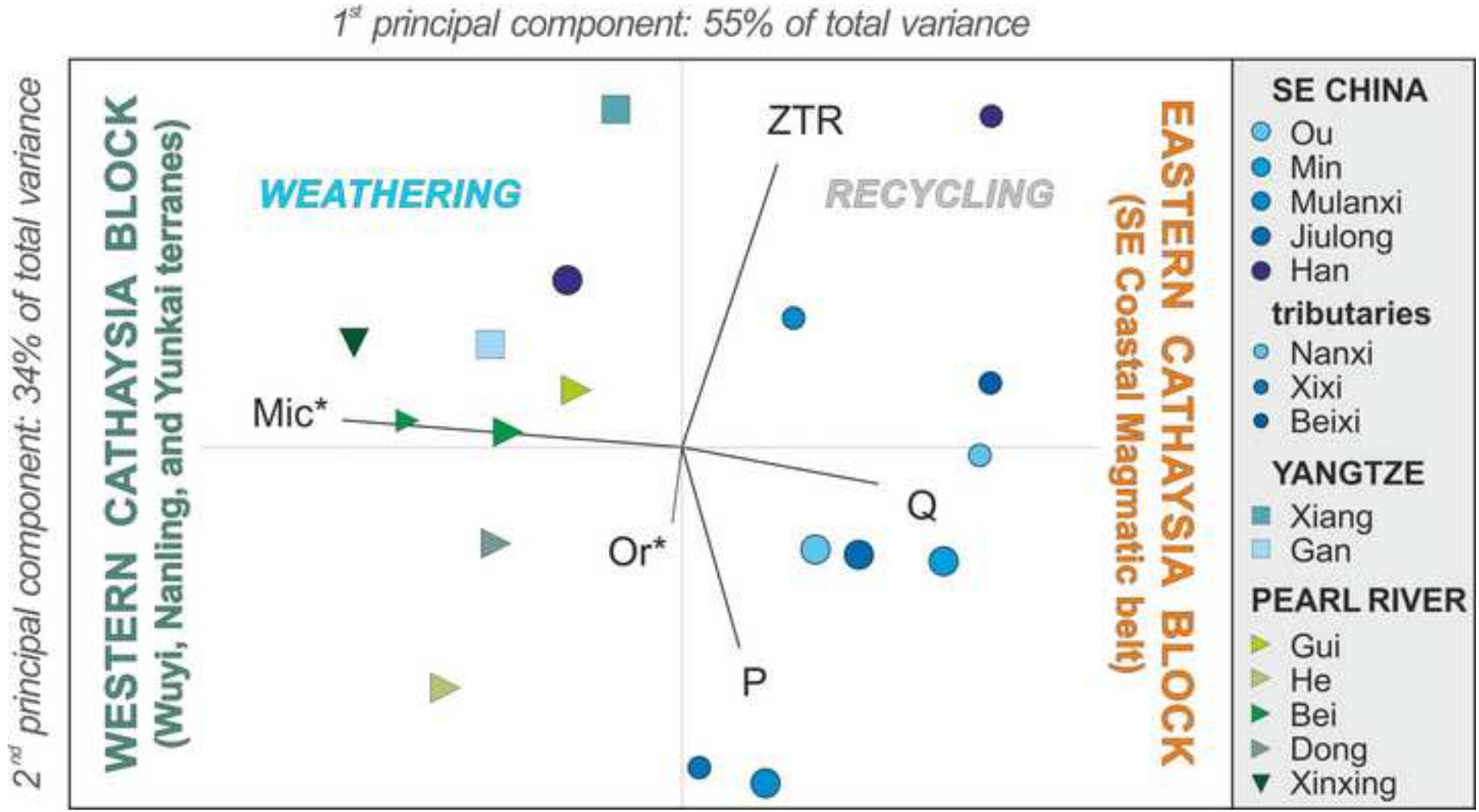

Figure 12

Click here to download high resolution image

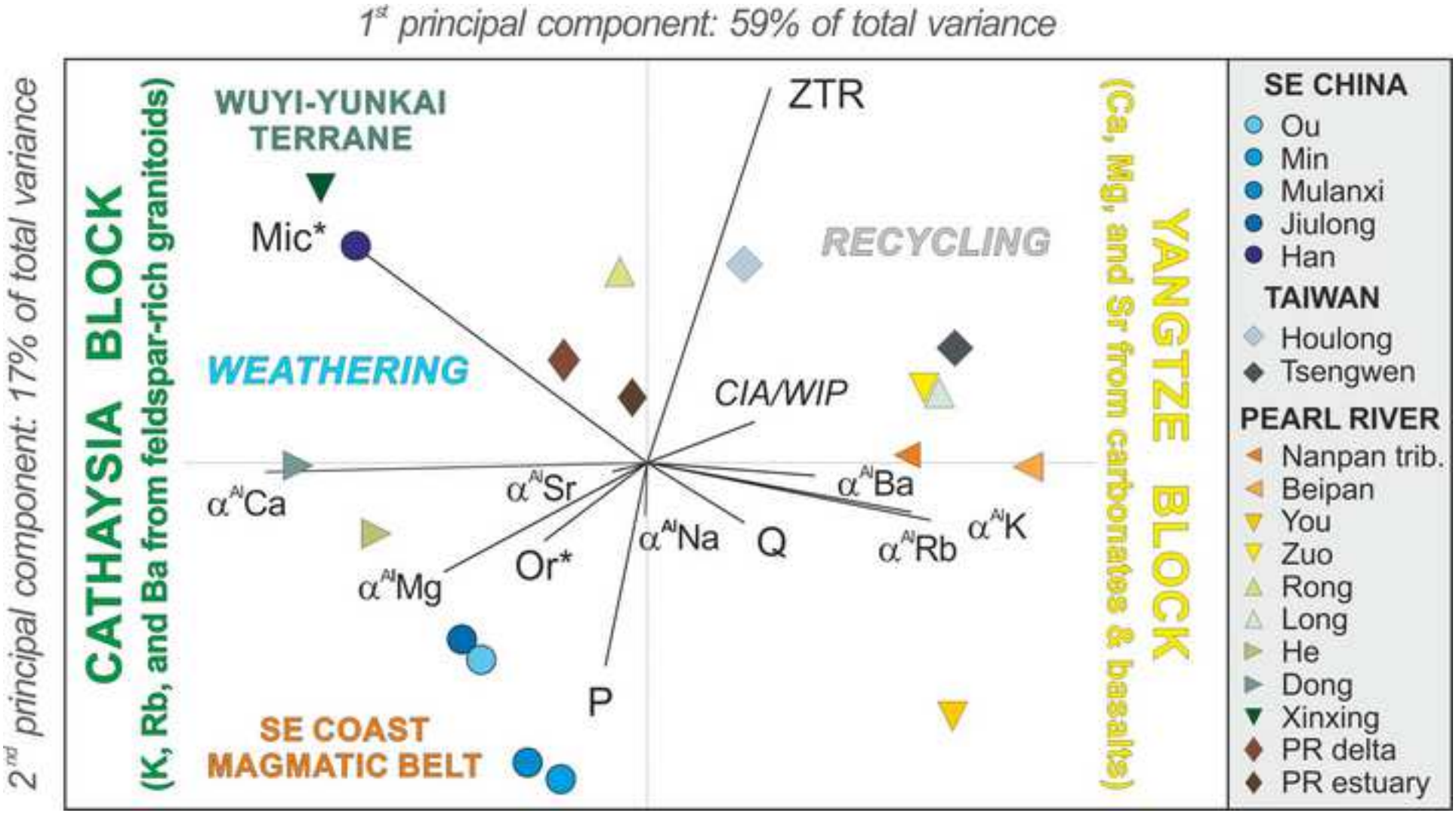

Table 1

Click here to download Table: Table 1 PearlProv Rivers.xlsx

Rivers	Drainage area (10^3 km^2)	Length (km)	Water discharge (km^3/yr)	Suspended load (10^6 t/yr)	Sediment yield (t / km^2/ yr)	Erosion rate (mm/yr)
PEARL RIVER						
Nanpan	56.8	914	21.7	7.0	135	0.05
Beipan	26.6	449	12.3	12.3	509	0.19
Hongshui	52.6	659				
TOTAL HONSHUI	**136.0**	**1573**	**69.6**	**45.6**	**369**	**0.14**
Rong	21.6	218	25.6	2.8	145	0.05
Long	16.4	367	12.7	1.5	97	0.04
TOTAL LIU	**57.2**	**773**	**58.8**	**6.5**	**124**	**0.05**
Qian	**198.0**	**1694**	**135**	**52.1**	**289**	**0.11**
You	38.6	707	17.2	5.5	157	0.06
Zuo	32.1	539	17.4	3.2	110	0.04
TOTAL YU	**90.7**	**1179**	**47.9**	**16.3**	**198**	**0.07**
Xun	**308.2**	**1866**	**229.3**	**33.5**	**119**	**0.04**
Gui	19.3	426	17.5	2.8	158	0.06
He	11.5	352	6.4	1.5	147	0.06
Xi	**329.7**	**2074**	**202.5**	**45.7**	**152**	**0.06**
Xinxing	2.4	145	1.2	n.d.	n.d.	n.d.
Bei	46.7	468	51.0	12.7	299	0.11
Dong	35.3	562	25.7	6.9	216	0.08
TOTAL PEARL	**450**	**2320**	**280**	**65**	**160**	**0.06**
COASTAL SE CHINA						
Han	30.1	470	24.5	6.9	253	0.09
Jiulong	14.7	258	14.1	2.5	184	0.07
Mulanxi	1.7	168	1	0.5	304	0.11
Min	61.0	577	56.1	8.2	149	0.06
Ou	18.0	390	20.2	2.7	165	0.06
YANGTZE BASIN						
Wu	115.7	1037	52.0	17.0	162	0.06
Yuan	89.2	1022	68.4	17.6	217	0.08
Xiang	94.7	948	72.2	11.4	132	0.05
Gan	83.5	766	68.7	9.9	130	0.05
TAIWAN ISLAND						
Houlong	0.5	58	1.4	3.3	7260	2.72
Bazhang	0.5	81	0.7	2.6	5720	2.14
Tsengwen	1.2	138	1.1	23.0	21083	7.90

Table 2

Click here to download Table: Table 2 PearlProv Data.xlsx

	n°	Q	F	Lvm	Lc	Lsm	Lm	P/F	Mic*/F	tHMC	ZTR	Ep	Grt	CSKA
PEARL RIVER														
Hongshui	3	31	3	18	12	36	0	47%	5%	0.1	25	7	0	0
Yu	3	60	7	5	7	20	1	55%	2%	0.5	30	11	3	0
Liu	3	77	10	2	0	8	2	50%	6%	0.2	41	18	1	0
Gui + He	2	66	23	2	2	6	2	34%	11%	0.1	18	11	6	1
Bei + Dong + Xinxing	4	69	23	1	0	5	2	29%	18%	0.3	32	16	5	17
Xi River	2	54	16	1	3	23	2	56%	13%	0.3	27	17	1	1
Pearl River mouth	4	70	20	2	0	7	1	44%	8%	0.3	37	18	5	2
SE CHINA														
Jiulong + Han	5	77	18	4	0	1	0	41%	6%	0.6	26	33	8	1
Ou + Min + Mulanxi	5	53	20	23	0	1	2	59%	2%	0.9	13	61	3	2
YANGTZE BASIN														
Wu	1	34	2	7	18	40	0	50%	0%	0.1	17	17	12	0
Yuan	1	48	6	7	1	36	1	58%	6%	0.1	44	27	1	0
Xiang+Gan	2	77	18	1	0	3	1	26%	18%	0.3	55	13	5	1
WEST TAIWAN	3	64	9	2	3	21	0	68%	5%	0.2	52	13	15	2

Table 3

Click here to download Table: Table 3 PearlProv Lithologies.xlsx

Rivers	Area (10^3 km^2)	Granite	Schist	Basalt	Carbonat	Sandstone
Pearl River tributaries						
Nanpan	56.8	4%	4%	26%	16%	26%
Beipan	26.6	0%	0%	26%	24%	27%
HONGSHUI	136.0	3%	2%	18%	33%	24%
You	38.6	6%	0%	10%	28%	26%
Zuo	32.1	2%	0%	2%	56%	33%
YU	90.7	7%	0%	6%	32%	37%
Rong	21.6	5%	38%	0%	23%	32%
Long	16.4	0%	8%	0%	77%	10%
LIU	57.2	2%	19%	0%	55%	21%
Gui	19.3	3%	0%	0%	54%	43%
He	11.5	27%	3%	0%	29%	19%
Xinxing	2.4	44%	12%	0%	32%	3%
Bei	46.7	32%	3%	0%	38%	13%
Dong	35.3	44%	10%	0%	9%	26%
Pearl River						
Qian	198	3%	7%	12%	40%	23%
Xun	308.2	5%	5%	10%	36%	28%
Xi	329.7	13%	5%	7%	33%	27%
Coastal SE China						
Han	30.1	45%	14%	0%	6%	23%
Jiulong	14.7	53%	4%	0%	4%	27%
Mulanxi	1.7	44%	3%	0%	0%	28%
Min	61	37%	29%	0%	1%	19%
Ou	18	40%	32%	0%	0%	19%
Yangtze tributaries						
Wu	115.7	0%	1%	5%	45%	24%
Yuan	89.2	1%	22%	1%	22%	40%
Xiang	94.7	13%	12%	1%	19%	34%
Gan	83.5	15%	25%	1%	7%	38%

Appendix Tables

Click here to download Background dataset for online publication only: Appendix A PearlProv.xlsx

Interactive Map file (.kml or .kmz)

Click here to download Interactive Map file (.kml or .kmz): PearlProv.kmz

Conflict of Interest Statement

The authors declared that they have no conflicts of interest to this work. We declare that we do not have any commercial or associative interest that represents a conflict of interest in connection with the work submitted.